Elsevier Editorial System(tm) for Marine and Petroleum Geology

Manuscript Draft

Manuscript Number: JMPG-D-19-00122R3

Title: Permeability distribution and scaling in multi-stages carbonate damage zones: insight from strike-slip fault zones in the Tarim Basin, NW China

Article Type: Full Length Article

Keywords: Carbonate damage zone; Permeability; Scaling; Fracture; Diagenesis

Corresponding Author: Dr. guanghui wu,

Corresponding Author's Institution: Southwest Petroleum University, China

First Author: guanghui wu

Order of Authors: guanghui wu; Qu haizhou; kunzhi Zhao; Nicola Scarselli; Yintao Zhang; Jianfa Han; Yifeng Xu

Abstract: Architecture and permeability of fault damage zones are important for understanding fault mechanisms and fluid flow in fractured rocks. Nevertheless, this understanding is often hindered by limited availability of data, especially in the subsurface. A comprehensive suite of cores, logs and production data is here presented to unravel petrophysical properties and fracture characteristics of deep (> 6000 m) Ordovician limestones within strike-slip fault zones of the Tarim intracratonic basin (NW China). The results show that (1) the carbonate porosity is mainly secondary dissolution porosity and comprises low porosity (< 5%) and low permeability (< 0.5 mD) of the matrix reservoirs, and the "sweet spots" in fractured reservoirs with high permeability (> 5 mD) and high porosity (> 8%); (2) the fault damage zones are generally tight with fracture aperture < 0.05 mm that formed during multiple genetic events and were successively affected by marked diagenesis; (3) the fracture porosity is negligible, but fracture related dissolution is of critical significance and enhance permeability by more than two orders of magnitude higher than the tight matrix reservoirs in fault damage zones; (4) fracture attributes (frequency and aperture), permeability and production across fault zones display a distinct dichotomy between the inner and outer damage zones, with high permeability and production mainly within 500 m of inner damage zones; (5) the permeability had no distinct logarithmic or power-law scale to distance to fault, but a large scatter and slow decrease in inner damage zones. The results indicate that in deep subsurface carbonate reservoirs along fault zones of the Tarim basin, (1) permeability can be characterized by integrating cores, log and production data at different scales; (2) multi-stages fracture diagenesis, particularly of the late stage fracturing and fracture related dissolution, dominated the permeability in the carbonate damage zones; (3) an increased cementation and fracture diagenesis of fault cores led to a scattered permeability distribution in the inner damage zones; (4) "sweet spots" of fractured reservoirs are main exploitation targets along the fault damage zones.

Research Data Related to this Submission

Title: Data for: Architecture and permeability in tight carbonate damage zone in the Tarim Basin, NW China
Repository: Mendeley Data
https://data.mendeley.com/datasets/d2zygkrys4/draft?a=a90c2763-1d06-4f7e-84c0-a651af96105b

Highlights

1. Permeability across fault zones in tight carbonate rocks.

2. A distinct dichotomy between the inner and outer damage zones with fracture attributes and permeability and production.

3. Large scattered permeability in inner damage zones.

4. Diagenesis dominated the permeability in the carbonate damage zones.

Permeability distribution and scaling in multi-stages carbonate damage zones: insight from strike-slip fault zones in the Tarim Basin, NW China

Guanghui Wu[a,b*], Kuanzhi Zhao[c], Haizhou Qu[a], Nicola Scarselli[d], Yintao Zhang[c], Jianfa Han[c*], Yifeng Xu[a]

[a] *School of Geoscience and Technology, Southwest Petroleum University, Chengdu 610500, China*

[b] *Southwest Petroleum University, Division of Key Laboratory of Carbonate Reservoirs, CNPC, Chengdu, 610500, China*

[c] *PetroChina Tarim Oilfield Company, Korla 841000, China*

[d] *Department of Earth Sciences, Royal Holloway University of London, Surrey TW200EX, United Kingdom*

Abstract

Architecture and permeability of fault damage zones are important for understanding fault mechanisms and fluid flow in fractured rocks. Nevertheless, this understanding is often hindered by limited availability of data, especially in the subsurface. A comprehensive suite of cores, logs and production data is here presented to unravel petrophysical properties and fracture characteristics of deep (> 6000 m) Ordovician limestones within strike-slip fault zones of the Tarim intracratonic basin (NW China). The results show that (1) the carbonate porosity is mainly secondary dissolution porosity and comprises low porosity (< 5%) and low permeability (< 0.5 mD) of the

matrix reservoirs, and the “sweet spots” in fractured reservoirs with high permeability (> 5 mD) and high porosity (> 8%); (2) the fault damage zones are generally tight with fracture aperture < 0.05 mm that formed during multiple genetic events and were successively affected by marked diagenesis; (3) the fracture porosity is negligible, but fracture related dissolution is of critical significance and enhance permeability by more than two orders of magnitude higher than the tight matrix reservoirs in fault damage zones; (4) fracture attributes (frequency and aperture), permeability and production across fault zones display a distinct dichotomy between the inner and outer damage zones, with high permeability and production mainly within 500 m of inner damage zones; (5) the permeability had no distinct logarithmic or power-law scale to distance to fault, but a large scatter and slow decrease in inner damage zones. The results indicate that in deep subsurface carbonate reservoirs along fault zones of the Tarim basin, (1) permeability can be characterized by integrating cores, log and production data at different scales; (2) multi-stages fracture diagenesis, particularly of the late stage fracturing and fracture related dissolution, dominated the permeability in the carbonate damage zones; (3) an increased cementation and fracture diagenesis of fault cores led to a scattered permeability distribution in the inner damage zones; (4) “sweet spots” of fractured reservoirs are main exploitation targets along the fault damage zones.

Key words： Carbonate damage zone; Permeability; Scaling; Fracture; Diagenesis

1. Introduction

Fault zones significantly influence the mechanical, hydraulic and permeability properties of the host rocks (e.g., Caine et al., 1996; Kim et al., 2004; Faulkner et al., 2010; Bense et al., 2013). Permeability variations due to faulting can extend across hundreds of meters in fault zones (including fault core and damage zone) making these a critical element of the evolution of faults and strongly affecting fluid migration and accumulation in sedimentary basins (e.g., Aydin, 2000; Tondi, 2007; Pei et al., 2015). Permeability in fault zones may display a power–law relationship with distance to fault core, consistent with fracture frequency increase toward fault (e.g., Mitchell and Faulkner, 2009; Torabi et al., 2018). On the other hand, permeability generally presents strong heterogeneity and anisotropy along and across fault zone because of (1) the different types host rocks, (2) extent of faulting and associated fracturing, and (3) diagenesis, with the latter particularly relevant for carbonate rocks (e.g., Billi et al., 2003; Micarelli, E., 2006; Agosta et al., 2007; Rotevatn and Bastesen, 2012; Haines et al., 2016; Wu et al., 2019b). In carbonate fault zones, permeability vary with lithology, sedimentary facies and strata thickness (e.g., Agosta et al., 2012; Guerriero et al., 2013; Afşar et al., 2014; Michie, 2015; Haines et al., 2016), and vary substantially with fracture attributes (frequency, length, aperture), architecture and linkage (e.g., Rotevatn and Bastesen, 2012; Korneva et al., 2014; Brogi and Novellino, 2015; Haines et al., 2016; Torabi et al., 2018; Balsamo et al., 2019; Ferraro et al., 2020). In addition, hierarchical fracture systems characterized by specific geometrical features

present different permeability in carbonate reservoirs (e.g., Guerriero et al., 2013, 2015). During long burial, diagenesis (e.g., cementation and dissolution) drastically modifies permeability of fault damage zones as these structures grow through time (e.g., Billi et al., 2003; Hausegger et al., 2010; Haines et al., 2016; Williams et al., 2017). High level of fracturing in fault damage zones is thought to enhance significant diagenetic modifications during burial (Olierook et al., 2014; Arosi and Wilson, 2015; De Graaf et al., 2017). Due to sparse permeability data gained from strong heterogeneous fault zones, there is poor understanding on the permeability scaling with distance to fault, and how architecture, diagenesis and permeability of carbonate fault damage zones are interrelated in sedimentary basins.

Large oil and condensate fields in China have been found in carbonates of the Tarim Basin (Du, 2010; Lu et al., 2017). These Ordovician carbonate reservoirs are generally classified into reef-shoal and paleo-karst reservoirs and are controlled by microfacies and karstification, respectively (Du, 2010; Zhao et al., 2012; Yang et al., 2014; Shen et al., 2015; Li et al., 2018; Zhang et al., 2018). In recent years, hydrocarbon exploration and production has focused on cavity reservoirs related to fault damage zones (Wu et al., 2016, 2019a; Lu et al., 2017; Neng et al., 2018; Tian et al., 2019; Méndez et al., 2020; Yang et al., 2020). However, lateral and vertical heterogeneities result in complex production responses along these fault damage zones, posing a challenge for the exploitation of these carbonate reservoirs. The architecture and permeability of fault damage zone in the subsurface, which is of great importance for the reservoirs, have not been specifically addressed.

In this paper, cores, thin sections and well log data are used to feature the internal structures of the fault damage zones in the Ordovician carbonates of the Tarim Basin. By gathering fracture attributes (e.g., dip angle, azimuth, aperture and frequency) from wells data at variable distance from faults, we further examine the relationship between fracture attributes and increasing separation from faults. Integration of well log data, cores and productions permitted a multi-scale appreciation of permeability along fault damage zones. Finally, we discuss the controlling factors on permeability and on fault damage zones growth in sedimentary basins.

2. Geological setting

The Tarim Basin extends for of 560 000 km^2 making it the largest petroliferous basin in China (Fig. 1). This intracratonic basin contains Archean-Early Neoproterozoic crystalline basement covered by a ~15 km thick, Late Neoproterozoic-Quaternary succession (Fig. 1b; Jia, 1997). The Tarim Basin experienced a multi-stage tectonic evolution, accompanied by the creation of an intricate network of fault systems (e.g., Jia, 1997; Tang et al., 2014; Li et al., 2016; Wu et al., 2016, 2019a; Lu et al., 2017; Deng et al., 2019). The Halahatang area, which is the focus of this research, extends over an area of ~8000 km^2 and is located in the southern slope of the Northern Uplift (Fig. 1). Here, a continuous, basal carbonate succession of Cambrian dolomite transitioning to Upper Ordovician limestones is overlain by Silurian-Cretaceous and Cenozoic thick siliciclastics (Fig. 1b). The Middle-Upper Ordovician

carbonate reservoirs (Fig. 2a) are buried at depth ranging 6500-8000 m and gently dipping to the south of the basin (Fig. 1b).

In recent years, 3D seismic data has allowed to identify a prominent conjugate set of strike-slip faults that developed in the Cambrian-Ordovician (Fig. 2b; Wu et al., 2019a). These were reactivated in the Silurian-Permian and in the Meso-Cenozoic, forming large flower structures (Fig. 3). Fault zone length is generally up to 70 km with maximum apparent throw along faults less than 150 m at the Ordovician carbonates level (Figs. 2b and 3b; Wu et al., 2019a, 2020). Generally, these faults form positive flower structures with transpressional horsts in the Ordovician carbonate rocks (Fig. 3). A set of seismic attributes, such as seismic coherence and curvature, were implemented to identify and map the fault damage zone (including fault core) in 3D seismic datasets (Wan et al., 2016; Wu et al., 2019a, 2020). The cumulative data of fracture frequency, aperture and production data were used to constrain width of damage zones (Wu et al., 2019a). These results showed that the fault damage zones are stripped and fan-shaped with widths in the range of 1000-3000 m along faults (Fig. 2b). This width range overlaps with zones of enhanced hydrocarbon production within ~1200 m from fault zones (Wu et al., 2019a). Also, more than 200 wells drilled in the Ordovician carbonate reservoirs have attested high production rates when located within fault damage zones.

In this study area, The Middle-Upper Ordovician carbonate reservoirs can reach thickness in excess of 300 m and are mainly formed by shallow shoal facies developed in a broad ramp platform (Fig. 2a ; Du, 2010; Gao et al., 2015). These

facies are mainly grainstones to wackstones and small reefs (Figs. 4a-4d; Du et al., 2010; Wu et al., 2019b) that formed large shoal sections interbedded with inter-shoal mudstones, often found to be karstified (Du et al., 2010). From a reservoir standpoint, these are tight carbonates that have very low matrix porosity (< 8%), and low permeability (< 5 mD) and considerable lateral and vertical heterogeneity. It is assumed that when production from these reservoirs exceeds 10 Mbbl/yr they are located by fault damage zones.

3. Methods

Based on data from a large set of 50+ wells penetrating the Ordovician carbonates, we compiled a database of borehole cores, thin sections and well logs to describe the architecture of fault zones. The geometric and porosity features of fracture, pore (diameter < 2 mm), vug (diameter between 2-100 mm) and cavity (cavity diameter > 100 mm, large cavity diameter > 1000 mm) were documented in cores and thin sections, as well as in well log data (Fig. 4). Due to the sparse and discontinuous nature of core and thin section data, fracture attributes of frequency, dip angle, aperture and filling were measured from log data only (Wu et al., 2019a). Micro-resistivity image logging images (FMI) allowed detailed fracture identification, with dip angle and azimuth determination from 64 wells. The fracture frequency is the average number of fractures per meter in a well. Horizontal stylolite was excluded in the compiled data, as well as small fractures less than 5 cm in length for which identification was ambiguous.

Petrophysical properties were measured from 1181 core plugs from 46 wells. The porosity and permeability were measured by liquid saturation method and gas measurement method with klinkenberg-correction, respectively (e.g., Du, 2010; Yang et al., 2020). In 49 wells, porosity was mainly interpreted by volume model from density log data, whereas fracture porosity was derived from dual-lateral log interpretation model (Du et al., 2010; Tian et al., 2019). The permeability was constrained by an empirical equation from matrix porosity-permeability plots of core plugs data (Liu et al., 2009; Yang et al., 2020) as well as from production tests using the pressure decline method (Sivey and Lee, 2013; Wan et al., 2018). In addition, we collected oil production data from 196 wells. Although there is some uncertainty in the use of oil production as proxy for permeability, it is suggested that this is a valuable method to investigate permeability in heterogeneous carbonate reservoirs (Wu et al., 2019a).

Structural maps created by interpreting seismic data were used to measure distance between wells and adjacent major faults (Wu et al., 2019a). Eleven major faults were mapped from seismic data by using seismic sections and attributes like coherence and curvature (Fig. 2b). Small faults with length < 5 km were excluded from the analysis. Directional survey was utilized to take into account trajectories of deviated wells. This survey, however, might carry an error of up to 100 m from the actual location of the wellbore. Fracture attributes and petrophysical properties of country rock are measured from wells with variable distance from major faults. This allowed exploring the variation of these properties within fault damage zones.

Fracture attributes and permeability data are listed in the Supplementary material.

4. Results

4.1. Carbonate porosity

In the study area, unfractured cores have little visible porosity (Fig. 4a), and only a few dissolution vugs occurred in the Ordovician carbonates (Fig. 4b). The intergranular pores are almost lost by multiple calcite cements (Fig. 4c). More than 80% porosity is of intergranular dissolution porosity, and some intragranular and intercrystalline dissolution porosity (Figs. 4c and 4d). In reef limestones and grainstones, intragranular porosity are generally residual micropores (diameter < 10 μm). Grains floating in the cements suggest a high primary porosity (Fig. 4c). By observing cores and thin sections, most dissolution porosity in the rock occurred along the fractures (Figs. 4-6).

Except for pervasive horizontal stylolites, fractures in the fault zones developed mainly in 1-2 sets with high dip angle (Figs. 4-6). In places, oblique and en echelon fractures are observed in cores (Fig. 6b) and thin sections. A similar arrangement is observed at the seismic scale for faults. This self-similarity is also showed in conjugate fractures (Figs. 4e and 6g) interpreted in FMI images. It is worth noting that some fractures display late enlargement and reactivation (Figs. 6c, d, i), suggesting multiple phases of fracture activity. Open fractures are generally late micro-fractures that cut across older fractures (Figs. 6f, h) and late reactivated fractures (Figs. 6c, i).

Multiple diagenetic events of cementation and dissolution affecting fractures have been identified, suggesting the occurrence of at least three cycles of fracture reactivations (Wu et al., 2019b). These fractures are mainly filled by calcite precipitations, and some exhibit bitumen and argillaceous fillings (Figs. 5-6). Intense and multiple phases of cementations have resulted in sparse residual fracture porosity (< 20%). In the fractured reservoirs, dissolved pores and vugs along fractures are commonly observed in cores, thin sections and FMI images (Figs. 4d, 4e, 6c-e). This is remarkably different from sparse dissolution porosity of the country rocks (Fig. 4a). Importantly, most of the dissolution porosity is coincident with the late fractures (Figs. 6f and 6i), but some dissolution porosity is preserved along cement bridges in the fractures (Fig. 6j).

High production is commonly from large cavity reservoir that in seismic reflection profiles are identified by “bead-shape” features (Fig. 4g; low frequency and high-amplitude reflections). Although their origin is still debated (Du, 2010; Yang et al., 2013), these cavities are commonly found along fault damage zones. With cores hardly obtained from large cavities, high mud loss, abnormal drilling breaks and mud overflow all indicate that many wells encountered large cavities during drilling. For example, mud loss in H6-2 reached up to 1500 m^3. Large cavities are also characterized by enlarged borehole diameter, raised natural gamma, and reduced resistivity in well log data (Fig. 4f).

Consequently, the porosity of the Ordovician carbonate is mainly of secondary fracture, pore, vug and cavity along fault zones.

4.2. Internal structure

4.2.1. Internal structure of fault core

Few wells have penetrated large fault cores, but some penetrated secondary, small faults part of damage zones of major structures. Cores data in fault cores show carbonate breccias and cataclastic rocks filled with a fine-grained matrix (Figs. 5a and 5b). Some collapse breccia show some degree of abrasion, which resulted in smaller particles (Fig. 5b). The fine matrix fillings of ultracataclasite and gouge developed between breccias. Further, some of the fault cores exhibit multiple cements and bitumen filling indicating multi-stage diagenesis (Figs. 5c and 5d). Two stages of calcite precipitated in micro-faults, with earlier, wide cements in the center separated by narrow fine cements on the walls (Fig. 5d). Multiple calcite precipitation is also observed in wide fractures suggesting high porosity and permeability could have had originally coexisted with fracture opening. In the fault cores, porosity is almost fully filled by cements (Figs. 5a, c, d) some gouges (Fig. 5b) and dry bitumen (Fig. 5c), but a little remnant of dissolution porosity (Fig. 5d).

Fault cores possibly have undergone multiple phases of diagenesis (Fig. 5), consistent with multiple phases of fault activation (Fig. 3). Furthermore, there are marked filling of multiple calcite cements and veins (Figs. 5c and 5d), which probably occurred as a response of a complex diagenetic history (Wu et al., 2019b).

4.2.2. Internal structure of damage zone

Except for localized folding, fault damage zones in the Ordovician carbonate comprise intense fracturing along the strike-slip faults (Figs. 6 and 7). Width of fault damage zone can be in excess of 1000 m (Wan et al., 2016; Wu et al., 2019a). The zone can be divided into an inner and an outer damage zones by their differing fracture frequency and local strain (de Joussineau and Aydin, 2007; Choi et al., 2016). Although the boundary of inner/outer damage zones is hard to be identified in the subsurface, seismic profiles show typical chaotic to discontinuous seismic facies in inner damage zones (Ma et al., 2019).

The inner zones flank the fault core, often exhibit a high fracture frequency and are formed by breccias and cataclastic rocks (Figs. 4d, 6a and 6e). The carbonate breccias have smaller size, more prominent edges, less abrasion and rotation than those found in fault cores. They are supported by grains, with little fine matrix materials. Cataclastic rocks, in general, are found to be finer in grain size and more angular than breccias (Figs. 4d, 6a and 6e). Multiple sets of fractures occurred within inner damage zones with irregular and relatively short length (Figs. 6a, e, f). Regardless of intense cementation, dissolution porosity well developed in the breccias and cataclastic rocks (Figs. 4d, 6a, 6d and 6e).

The outer damage zone is characterized by one or two sets of high dip angle fractures with sparse cataclastic rocks (Fig. 6i). The outer damage zone can be possibly distinguished from inner zone by a lesser fracture frequency, high dip fracture angle and narrow fracture aperture. This is consistent with other studies on fault

damage zones elsewhere (e.g., de Joussineau and Aydin, 2007; Choi et al., 2016). In addition, dissolution porosity and cements along fractures in outer damage zones is markedly less than in inner damage zones, suggesting a lower porosity. These weakly deformed zones can be identified from image logs and cores rather than seismic profiles. In the subsurface, the identification of the boundaries of inner and outer damage zones is challenging.

4.3. Fracture attributes in fault damage zones

4.3.1. Fracture occurrence and aperture

Fractures (excluded stylolites and induced fractures) varied in a large range of dip angles in cores (Fig. 6) and FMI images (Fig. 4e). FMI images from 64 wells indicate that the fracture dip angles vary from 20º to 90º (Fig. 7a). The data show a possible progressive increase of fracture dip angle with distance from fault when the distance is more than 400 m, but scattering of dip angles is large within 400 m from the fault core. Most wide aperture (> 0.05 mm) fractures have relatively high dip angles (> 75º). Similarly, fracture dip also varied in a wide range, particularly close to fault cores. There are two major sets of dipping fractures at N290º -N340º and N110º - N180º (Fig. 7b). Most fractures have low angles to the NNE trending faults, suggesting more fractures in NNE faults than in NNW faults in this conjugate fault system. Also, the peak azimuth varies with the location along the fault zone. Similar to fracture dip angle, there are more fractures in with a NE trend. In addition, the smaller

fracture azimuth varied largely, particularly close to fault core.

Measurements from cores indicated mean aperture values of 0.1-0.5 mm, with a few apertures in excess of 10 mm. We observed in cores that (1) the wider aperture fracture generally have larger length; (2) narrow fractures are usually in a range of 5-30 cm in length; and (3) the length of wide vertical fractures is in excess of 1 m. In thin sections, the aperture values generally vary in a range from 0.01mm to 0.5 mm. Because of cements filling, however, open aperture values concentrated in a narrow range from 0.01 to 0.04 mm. In FMI data (Fig. 7c), open aperture ranges from 0.001–0.07 mm with a few wider fractures of ~0.2 mm in width. These results suggest that most fractures have narrow open aperture. Notably, the fracture aperture values have two distinct decreasing trends with distance from fault (Fig. 7c): 1) for increasing distance up to 500 m, and 2) for distances > 500 m; regardless of the scatter of the data.

4.3.2. Fracture frequency

Due to sparse and scattered fractures measurements from cores and thin sections (Wu et al., 2019a), average fracture frequency was estimated by using FMI data from 64 wells. The background value of the fracture frequency is generally < 1 fractures/100 m and more than 5 fractures/m in fractured intervals. The mean fracture frequency varies largely from 0 to 84.5 fractures/100 m, with the high frequencies found in wells close to faults (Fig. 7d). Even though fractures were affected by faults with different size, fracture frequency generally decreases quickly from the fault cores

to the country rocks. This distribution is similar to the one found for siliciclastic rocks (Mitchell and Faulkner, 2009; Savage and Brodsky, 2011; Choi et al., 2016). Our data also suggest a larger scatter of two orders magnitude and a lower coefficient (R^2 =0.33). When compared with fault maps derived from seismic, it is found that some exceptional high fracture frequency values are associated to wells close to secondary fault splays (Fig. 7d). Importantly, fracture frequency decreased quickly with the distance from fault when the distance is more than 500 m from the fault. This means that two segments of the fracture frequency with distance to fault can be identified with a breakoff at ~500 m.

4.4. Permeability in fault damage zone

4.4.1. Permeability from core plugs

Core plug measurement (Fig. 8a) indicates that porosity and permeability of the Ordovician carbonates vary widely. The samples of unfractured rock have low porosity (in range of 0.11-8.97% and average of 1.26%) and low permeability (in range of 0.002-9.83 mD and average of 0.38 mD). Fractured carbonates have much higher porosity (in range of 0.29-13.48% and average of 2.19%) and permeability (in range of 0.02-452 mD and average of 24.8 mD). A strong positive correlation between porosity-permeability is observed in fractured and unfractured samples when porosity is > 2%. Plot of average porosity and permeability in a well against distance from fault shows a slight negative relationship (Fig. 8b). Most wells with high permeability (> 5

mD) are within a distance of 1.3 km from fault. The permeability and porosity present a decreasing trend with distance increasing above 500 m. However, porosity and permeability present a large scatter within a distance from faults of 500 m.

As for non-fractured lithologies (Fig. 9a), porosity from core plugs is slightly higher in grainstones than in pack/wackstons and mudstones. In fracture-bearing rocks, porosity is double in grainstones, and about 20-50% increase in pack/wackstones and mudstones when compared to non-fractured samples. Furthermore, permeability from fracture-bearing samples increases more than 25 times in grainstones and about 60 times in mudstones and pack/wackstones. In general, the Yijiangfang and Lianglitage formations have relatively higher porosity than the other formations, while the permeability in the Lower-Middle Ordovician is almost one order magnitude than the Upper Ordovician rocks (Fig. 9b).

The fracture-bearing samples (Fig. 9c) from oil-charged reservoirs have relatively higher porosity and permeability than those from dry reservoirs. Compared with non-oil and non-fractured bearing samples, permeability from the oil bearing samples increased up to two orders of magnitude and porosity increased about two times (Fig. 9c). Except for the fracture bearing but non-oil bearing samples, permeability from other samples shows a weak decline trend with depth in permeability (Fig. 9d).

4.4.2. Permeability from logging data

The carbonate reservoirs are generally divided into four types by porosity types

i.e., pore-vug, fracture–vug, cavity and fracture types (Du, 2010). Except for pore-vug type, other types are fracture-bearing reservoirs. Compiled electric log data from 256 reservoir intervals in 55 wells indicate that the reservoir thickness ranges 0.1-32 m with most being 0.4-8 m thick (Fig. 10).

In the dataset, porosity and permeability varied 3.8-85.9% and 0.44-25.68 mD in cavity reservoirs, 1.9-9.3% (avg. 3.5%) and 0.19-452 mD in fracture-vug reservoirs, 1.8-13.9% (avg. 3%) and 0.03-3.91 mD (avg. 0.51 mD) in pore-vug reservoirs, 0.1-2.1% and 0.06-381.6 mD in fracture reservoirs, respectively (Fig. 10a). The matrix reservoirs (pore-vug type) generally present low porosity (< 5%) and low permeability (< 1 mD), and a positive correlation between permeability and porosity. The fracture porosity of the reservoirs is low (0.01-0.77%), with most < 5% of the total porosity in the carbonate reservoirs. Other types of reservoir generally have higher permeability with up to 2 orders of magnitude than pore-vug reservoirs. High permeability intervals (> 2 mD) are typically fracture bearing intervals. In addition, some large cavities developed intervals that have much higher porosity (> 10%) and permeability (> 10 mD) despite being filled with breccia, calcite, and others.

Permeability and porosity form core plugs and log data are generally inconsistent (Fig. 10b). This suggests an intense vertical heterogeneity of the carbonate reservoirs. In plots of porosity/permeability vs. distance from fault (Figs. 10c and 10d), porosity and permeability are largely scattered within 500 m from fault, with a decreasing trend with increasing distances. This pattern is consistent with the data from the core plugs (Fig. 8b). Similar to core samples, permeability and porosity have a slightly decline

trend with increasing depths.

4.4.3. Permeability from production data

Due to large amount of drilling mud loss, there is generally an early completion of drilling at the top of the large cavity reservoirs, which are the major targets of oil exploitation in the Ordovician carbonates (Du, 2010). Consequently, permeability is mostly underestimated from the top of the reservoirs by cores and logging data, particularly in the highly fractured cavity reservoirs. In oil production vs. permeability plots, highly productive wells generally have high permeability (Fig. 11a; > 5 mD). Oil production data can give an indication of the relative bulk permeability of the producing formation in such heterogeneous reservoirs.

Similarly to fracture attributes, there is a decreasing trend of oil production with increasing distance from fault (Fig. 11b). When the distance from fault is more than 400 m, oil production presents a sharp decrease with increasing distances and a large scattered distribution within fault core. This is consistent with fracture frequency (Fig. 8b) and permeability data (Fig. 10d). It is noted that many production layers are facilitated by fracturing and show much higher permeability than that from logging data.

5. Discussion

5.1. Permeability indicators in heterogeneous carbonate damage zone

In homogeneous and some fractured rocks, permeability generally can be obtained from measurements in situ rocks and core plugs (e.g., Haines et al., 2016; Clarkson et al., 2019), and from interpretation of subsurface log data. In fractured rocks along fault zones, fracture attributes (e.g. frequency and aperture) could be a proxy for permeability of the in situ rocks. Due to significant heterogeneity and uncertainties around quality of fault permeability data, it is hard to measure bulk permeability directly in the intense heterogeneous rocks (e.g., Fisher et al., 2018; Debenham et al., 2019).

Multiple phases of tectonic and diageneis, together with complex secondary triple porosity and fracture and cavity formation (Figs. 5-7), imparted an extreme heterogeneity of the Ordovician carbonate reservoirs in the Tarim Basin (Du, 2010; Yang et al., 2020). Because of this, permeability from core plugs and log data are inconsistent with oil production data. Some wells characterized by high permeability from core and log data had actually low oil production; while wells yielding high production targets reservoirs with marked low permeability. Even for wells targeting similar highly permeable reef-shoal reservoirs, productions largely varied for three orders of magnitude and output fluctuated during production (e.g., Du, 2010; Yang et al., 2020). These inconsistencies could be generally related to intense heterogeneity as observed at different scales in the reservoirs analysed in this work, particularly for the

fractured ones.

In these heterogeneous reservoirs, fracture frequency has a poor relationship with permeability. Whereas, fracture frequency trend is consistent with the permeability trend derived from core plugs and log data. In the limit of the sampling methods, core plugs show a large range of permeability influenced by fractures and much lower matrix permeability (< 1 mD) in small scale rocks. The well log porosity and permeability are generally constrained by core plug data that are favorable for the reservoir interpretation near boreholes (Du, 2010), but cannot predict the heterogeneity of the reservoirs far away from the borehole, particularly the large fractured cavities. Stable production has a good correlation with permeability from Stoneley wave logging that can detect several meters away the boreholes (Fig. 11a; Du, 2010). Production data are consistent with core and log data in some cases, but generally not the highly fractured and heterogeneous reservoirs.

In this context, integration of core, well log and production data is key to reveal permeability from different scales in the subsurface. Considering the challenge in quantifying permeability from static data in heterogeneous reservoirs, oil production is a better proxy for permeability than core and log data.

5.2. Permeability distribution and scaling in carbonate damage zone

In this dataset, low permeability (< 2 mD) characters matrix (pore-vug type) reservoirs, but much higher permeability is encountered in fractured reservoirs (Figs.

8-10). The permeability values increased by fracturing are up to 2-5 orders of magnitude from core plugs, 1-4 orders of magnitude from log data and 1-3 orders of magnitude from oil production data. This suggests the permeability heterogeneity declines from small to large scale observations. When looking to vertical stratigraphic variations, the permeability in the Lower-Middle Ordovician rocks is higher up to one order of magnitude than in the Upper Ordovician rocks (Fig. 9b). This is consistent with higher production wells targeting the Lower-Middle Ordovician. Contrary to previous works that did not show correlation between porosity and permeability (Du, 2010), this research indicate that log data provide a good correlation for matrix (pore-vug) reservoirs (Fig. 10a). Also this work has highlighted that core plugs data indicate a good correlation between porosity and permeability for both fractured and unfractured reservoirs when porosity is > 2% (Figs. 8a). The porosity boundary at ~2% is probably related to the porosity types of pore and vug reservoirs. Permeability, in this case, presents a positive correlation with oil production (Fig. 11a).

In the study area, the extent of fault damage zones from faults has been constrained by plots of fracture frequency, cumulative fracture frequency, fracture aperture and production data and found to be 1100 m (Wu et al., 2019a). This study also shows a negative relationship between permeability and distance from fault in core plugs (Fig. 8b) and in logging data (Figs. 10c and 10d) as well as in oil production data (Fig. 11b). These trends are consistent with fracture frequency decreasing from fault core to host rocks as also shown in outcrop studies (e.g., de Joussineau and Aydin, 2007; Choi et al., 2016). However, this study presents a

dichotomy in this pattern across fault zone, which potentially divides fault damage zones into two parts: 1) an inner damage zone at distances up to 400-500 m, and 2) outer damage zones at distances > 500 m from fault (Figs. 7, 8, 10, 11). Permeability, together with oil production and fracture attributes, scatters widely and decreases slowly within 500 m in the inner damage zones. It is, however, striking that this decrement is significantly marked with distance from fault in the outer damage zones. This segmentation pattern is different from the continuous transition of permeability from inner to outer damage zones with a logarithmic or power-law scaling to distance reported by de Joussineau and Aydin (2007), Torabi and Berg (2018) and Debenham et al. (2019). Scattering of data in the inner damage zones might be possibly related to bias in the data and uncertainty related to fault interpretation from seismic. However, the occurrence of these two clear different trends suggests intricate and different evolution paths between the inner and outer damage zones.

5.3. Factors impact on permeability

5.3.1. Lithology

Lithology and microfacies can impact faulting and fracturing because of different mechanical and hydraulic properties, therefore influencing permeability along fault zones (Agosta et al., 2012; Afşar et al., 2014; Michie, 2015). Lithology and microfacies are also assumed to be of crucial significance in the Ordovician carbonate reservoirs in the Tarim Basin, particularly the reef-shoal reservoirs (Du, 2010; Zhao et

al., 2012; Yang et al., 2014; Shen et al., 2015; Zhang et al., 2018).

In this study area, primary porosity has been almost entirely occluded by strong cementation (Figs. 5 and 6). The grainstones did not show higher permeability than other lithological rocks (Fig. 9a). On the contrary, high permeability mudstones Fig. 9a) suggests that they are more subject to fracturing than the thick grainstones of the reef-shoal facies. On the other hand, there is similar permeability in the reef-shoal facies of the Yijianfang Formation and the inner platform of the Yingshan Formation, which have much higher permeability than the Upper Ordovician reef-shoal facies of the Lianglitage Formation (Fig. 9b; Du, 2010). This may indicate that permeability is unrelated to facies, but closely related to faulting and fracturing affecting these units.

In this context, there is little impact of lithology and microfacies on the permeability in the carbonates within fault zones of the Tarim Basin.

5.3.2. Fracturing

In tight rocks, permeability is significantly impacted by fracture frequency, aperture and roughness (Mitchell and Faulkner, 2009, 2012; Nara et al., 2011; Agosta et al., 2007, 2012; Meier et al., 2015). In addition, multiple fracture events may have a complex influence on fault permeability (Debenham et al., 2019).

The strike-slip fault systems affecting the Cambrian–Ordovician carbonates in the Tarim Basin were reactivated in the Silurian-Permian and Mesozoic-Eocene (Fig. 3). Early fractures are almost filled by cementation (Figs, 5c, 5d, 5f and 5g), while late

fractures are open (Figs. 6f, 6h) (Wu et al., 2019b). This suggests that the latter formed in the Paleogene account for most of the permeability of the carbonate reservoirs. As a result of multiple faulting events (Fig. 3), tectonic stresses can overprint carbonate textures, modifying porosity and ultimately increasing permeability (Storti et al., 2011; Balsamo et al., 2019). It is noteworthy that most fractures are NE striking (Fig. 7b), which is consistent with the NNE striking conjugate faults (Fig. 2b) and the NE striking in situ field stress (Wu et al., 2019a). Under a NE striking stress field in the Cenozoic, the NNE striking faults were reactivated, but not the NNW striking faults (Fig. 3). This led to enhanced activity and reactivation of the NE striking fractures. In addition, NE striking fractures are often open and wide in aperture, with aperture narrowing for fractures at different azimuths. All this is consistent with increased production for wells located along the NE striking faults.

Fracture frequency increasing permeability has been previously discussed in details (e.g., Wibberley and Shimanoto, 2003; Mitchell and Faulkner, 2012; Bauter et al., 2015). This phenomenon is further supported by the results of this study showing a distinct increase in permeability of 2-5 orders of magnitude in fractured reservoirs (Figs. 8, 9a and 9c). Across fault zones, there is a similar decreasing trend of permeability (Figs. 8b, 10d) and fracture frequency (Fig. 7d) with increasing distance from fault. Elsewhere in the study area fracture frequency has a poor correlation with permeability, suggesting the impact of other factors.

Generally, macrofractures control permeability at low effective pressure at shallow depths, while microfracture networks becomes more dominant in at depth (Nara et al.,

2011; Mitchell and Faulkner, 2012; Guerriero et al., 2015; Wang et al., 2016). The fractures affecting the deep carbonates of the study area have undergone a long history of diagenesis (Du et al., 2010), and resulted in their sealing by multiple filling events, particularly fractures with wide aperture (Figs. 5 and 6). Fracture aperture values from well log data (Fig. 7c) are generally smaller than 0.05 mm, which is much less than the values measured from cores and thin sections (Wu et al., 2019a). This suggests narrow open aperture of the fractures in the study area. This translates in a relatively low permeability (< 10 mD) in the reservoir intervals (Fig. 10a, d) in comparison with the fractured core plugs (Figs. 8a). This permeability values are four to six orders of magnitude less of those typically measured from outcrops of fractured rocks (Nara et al., 2011; Haines et al., 2016). This relatively low permeability of the carbonate of the Tarim Basin is possibly related to fracture roughness that can drastically lower permeability at depth (Huang et al., 2018 and references therein).

5.3.3. Diagenesis

With depths up to 7500 m, the Ordovician carbonates in the Tarim Basin show a slightly decrease of permeability with depth (Fig. 9d), suggesting that compaction had some negative impact on permeability. During the long burial history, the primary porosity of the Ordovician carbonates in the Tarim Basin was almost lost by cementation (Wu et al., 2019b) and present much lower permeability (< 1 mD) in matrix reservoirs than other reservoirs elsewhere (e.g., Billi et al., 2003; Haines et al.,

2016). More than 90% fracture porosity has been occluded by cementation as shown by cores and thin sections (Figs. 5, 6). In addition, the cementation varied largely amongst fractures and had a critical impact on developing a strong heterogeneity (Wu et al., 2019b), particularly in the inner damage zones (Fig. 6). Dissolution process of the carbonate reservoirs is common in the study area (Figs. 5, 6; Wu et al., 2019b). The dissolution porosity along fracture zones (Fig. 6e) may have enhanced permeability greatly, particularly for the large cavity reservoirs that have permeability more than 100 mD. Due to intense cementation of the carbonate reservoir, dissolution is crucial for enhancing porosity as well as permeability of these rocks. In addition, the oil-bearing fractures (Figs. 6a, c, d) have lower degree cementation and have higher porosity and permeability than none oil-bearing samples (Fig. 9c), suggesting that oil emplacement may be a key factor for preserving fracture opening and permeability.

In the fault damage zones, there are at least three stages of diagenetic processes following the fracture activities in the Ordovician carbonates (Figs. 5 and 6; Wu et al., 2019b). These diagenetic processes show a complex impact on the fault damage zones rather than a relatively uniform nature of diagenesis of the country rocks. In the breccia and cataclasite of the damage zones (including fault cores), the porosity and permeability are generally occluded by gouge and cements, consistent with the initiation of brecciation and cataclasis cannibalize fractures in the damage zone (e.g., de Joussineau and Aydin, 2007; Mitchell and Faulkner, 2009; O'Hara et al., 2017). Besides from the fact that cataclastic rocks developed close to fault cores, complex burial history and diagenesis might be also responsible for significant cementation in

such long-lived deformation zones. In this study, there is a stronger diagenesis (e.g. cementation) in the fault core than in the fault damage zone (Figs. 6 and 7; Wu et al., 2019b). On the other hand, many wells penetrated fractured cavities near the fault cores with varied oil productions (Fig. 11b), suggesting a strong and complicated dissolution and filling with variable permeability. Besides high production, many low permeability and low oil production wells occurred in inner damage zones which is in agreement with the findings that fault cores are typically made up of cataclastic rocks that are generally barriers to fluid flow in low-porosity rocks (Caine et al., 1996; Molli et al., 2010; Agosta et al., 2012). The complicated architecture and diagenesis could lead to a strong heterogeneous permeability along the fault damage zones, particularly of inner damage zones. Because of this, it is challenging to optimize well location in such complicated reservoirs along inner damage zones.

5.4. Factors influence the permeability between inner and outer damage zones

In this study, the permeability presents distinct boundary between inner and outer damage zones, and it is inconsistent with power-law scaling with distance from fault (Figs. 8b and 10d). Each segment is characterized by consistent values of fracture attributes (frequency and aperture) (Figs. 7c, 7d), particularly in the outer damage zones. This suggests that permeability variation between inner and outer damage zones is related to their relative fracture attributes (Torabi et al., 2018).

On the other hand, there is a poor correlation and different distribution pattern

between permeability and fracture attributes in the inner damage zones (Figs. 7, 8 and 10). Compared with a distinct fracture frequency decrease with distance from fault in inner damage zones (Fig. 7a), permeability (Figs. 8b and 10d) do not show obvious decline trend with distance. This might be related to the complex fracture network in inner damage zones, and contrasts with a relatively simple network of 1-2 sets of fractures in the outer damage zones. Different hierarchical fractures and their spatial networks and connectivity may considerably affect scattering of data in inner damage zones (Rotevatn and Bastesen, 2012; Guerriero et al., 2015).

Structural diagenesis shows a complex impact on the inner damage zones (Wu et al., 2019b). Breccia and cataclasite of the inner damage zones (including fault cores) show porosity and permeability generally occluded by gouge and cements (Fig. 6), consistent with brecciation and cataclasis that cannibalize fractures (e.g., de Joussineau and Aydin, 2007; Mitchell and Faulkner, 2009; O'Hara et al., 2017). Besides, from the fact that cataclastic rocks developed close to fault cores, complex burial history and diagenesis might be also responsible for significant cementation in such long-lived deformation zones. In this study, there is a stronger diagenesis (e.g. cementation) in the inner damage zones than in the outer damage zone (Fig. 6; Wu et al., 2019b). Thus, the permeability and production in inner damage zones do not show obvious decline trend with distance from fault. On the other hand, many wells penetrated fractured rocks in the inner damage zones with varying oil productions (Fig. 11b), suggesting a strong and complicated dissolution and cementation with variable permeability. Low permeability and low production wells are also found

amongst those targeting inner damage zones, this supports the findings that some cataclastic rocks are generally barriers to fluid flow in low-porosity rocks (Caine et al., 1996; Molli et al., 2010; Agosta et al., 2012). The complicated architecture and diagenesis could lead to a strong heterogeneous permeability along the fault damage zones, particularly in inner damage zones. Because of this, it is challenging to optimize well location in such complicated reservoirs along fault damage zones.

6. Conclusions

The integrated analysis of the Ordovician fractured reservoirs in the Tarim Basin presented in this study is summarized in the following conclusions.

1. Fault zones can be divided in a fault core that shows tight sealing due to calcite cementation, an inner damage zone with multiple sets of fractures affected by marked diagenesis, and an outer damage zone with two sets of high angle fractures. The boundary between inner/outer damage zones can be identified by abrupt changes of fracture attributes and permeability with distance from fault.

2. Evaluation of permeability in carbonate fault damage zones was constrained at different scales by the analysis of cores, log and production data. In the fault core in outer damage zones, permeability, fracture frequency and oil production present a decreasing trend with distance from faults, whereas large scattering of these values is a characteristic of first 500 m of inner damage zones.

3. Permeability of fault zones is up to two orders of magnitude larger than that found

in unfractured matrix reservoirs. Late fracturing and dissolution are the main controlling factors of permeability these carbonate reservoirs. Multiple faulting and diagenetic events have overprinted the complex permeability along the carbonate damage zones – these factors are crucial for permeability evolution and need further investigation.

4. High permeability "sweet spots" occur where cavity reservoirs develop. These seem to preferably align along the main fault damage zones and should be considered as the main target for future exploitation in the Tarim basin.

Acknowledgments

The authors thank the Tarim Oil Company for data support and project research. We are grateful to for the reviewers' comments of the manuscript that substantially improved the manuscript. We also thank Lijuan Zhang, Duoming Zheng, Chenshen Zhang, En Xie and Quan Cai for their help for data analysis and interpretation. This study has been partly supported by National Natural Science Foundation of China (Grant No. 41472103; 41702163) and Chinese National Science and Technology Major Project (2016ZX05004001).

References

Afşar, F., Westphal, H., Philipp, S.L., 2014. How facies and diagenesis affect

fracturing of limestone beds and reservoir permeability in limestone–marl alternations. Mar. Petrol. Geol. 57, 418–432.

Agosta, F., Prasad, M., Aydin, A., 2007. Physical properties of carbonate fault rocks, Fucino Basin (Central Italy): implications for fault seal in platform carbonates. Geofluids 7, 19–32.

Agosta, F., Ruano, P., Rustichelli, A., Tondi, E., Galindo-Zaldívar, J., Sanz de Galdeano, C., 2012. Inner structure and deformation mechanisms of normal faults in conglomerates and carbonate grainstones (Granada Basin, Betic Cordillera, Spain): inferences on fault permeability. J. Struct. Geol. 45, 4–20.

Arosi, H.A., Wilson, M.E.J., 2015. Diagenesis and fracturing of a large-scale, syntectonic carbonate platform. Sedimentary Geology 326, 109–134.

Aydin, A., 2000. Fractures, faults and hydrocarbon entrapment, migration and flow. Mar. Pet. Geol. 17, 797–814.

Bauer, J.F., Meier, S., Philipp, S.L., 2015. Architecture, fracture system, mechanical properties and permeability structure of a fault zone in Lower Triassic sandstone, Upper Rhine Graben. Tectonophysics 647-648, 132–145.

Bense, V.F., Gleeson, T., Loveless, S.E., Bour, O., Scibek, J., 2013. Fault zone hydrogeology. Earth-Sci. Rev. 127, 171–192.

Billi, A., Salvini, F., Storti, F., 2003. The damage zone-fault core transition in carbonate rocks: implications for fault growth, structure and permeability. J. Struct. Geol. 25, 1779–1794.

Brogi, A., Novellino, R., 2015. Low Angle Normal Fault (LANF)-zone architecture and permeability features in bedded carbonate from inner Northern Apennines (Rapolano Terme, Central Italy). Tectonophysics 638, 126–146.

Caine, S.J., Evans, J.P., Forster, C.B., 1996. Fault zone architecture and permeability structure. Geology 24, 1025–1028.

Choi, J.-H., Edwards, P., Ko, K., Kim, Y.-S., 2016. Definition and classification of fault damage zones: A review and a new methodological approach. Earth-Sci. Rev. 152, 70–87.

Clarkson, C.R., Vahedian, A., Ghanizadeh, A., Song, C.Y., 2019. A new low-permeability reservoir core analysis method based on rate-transient analysis theory. Fuel 235, 1530–1543.

Debenham, N., Farrell, N.J.C, Holford, S.P, King, R.C, Healy, D., 2019. Spatial distribution of micrometre‐scale porosity and permeability across the damage zone of a reverse‐reactivated normal fault in a tight sandstone: Insights from the Otway Basin, SE Australia. Basin Research 31, 640–658.

De Graaf, S., Reijmer, J.J.G. Bertotti, G.V., Bezerra, F.H.R., Cazarin, C.L., Bisdom, K., Vonhof, H.B., 2017. Fracturing and calcite cementation controlling fluid flow in the shallow-water carbonates of the Jandaíra Formation, Brazil. Mar. Petrol. Geol. 80, 382–393.

De Joussineau, G., Aydin, A., 2007. The evolution of the damage zone with fault growth in sandstone and its multiscale characteristics. J. Geophys. Res. 112, B12401, doi:10.1029/2006JB004711.

Deng, S., Li, H.L., Zhang, Z.P., Zhang, J.B., Yang, X., 2019. Structural characterization of intracratonic strike-slip faults in the central Tarim Basin. AAPG Bull. 103, 109–137.

Du, J.H., 2010. Oil and gas exploration of Cambrian-Ordovician carbonate in Tarim basin. Beijing：Petroleum Industry Press, 1–177 (in Chinese).

Faulkner, D.R., Jackson, C.A.L., Lunn, R.J., Schlische, R.W., Shipton, Z.K., Wibberley, C.A.J., Withjack, M.O., 2010. A review of recent developments concerning the structure, mechanics and fluid flow properties of fault zones. J. Struct. Geol. 32, 1557–1575.

Ferraro, F., Agosta, F., Prasad, M., Vinciguerra, S., Violay, M., Giorgioni, M., 2020. Pore space properties in carbonate fault rocks of peninsular Italy. J. Struct. Geol. 130, https://doi.org/10.1016/j.jsg.2019.103913.

Fisher, Q.J., Haneef, J., Grattoni, C.A., Allshorn, S., Lorinczi P., 2018. Permeability of fault rocks in siliciclastic reservoirs: Recent advances. Mar. Petrol. Geol. 91, 29–42.

Gao, Z.Q., Fan, T.L., 2015. Carbonate platform-margin architecture and its influence on Cambrian-Ordovician reef-shoal development, Tarim Basin, NW China. Mar. Petrol. Geol. 68, 291–306.

Guerriero, V., Dati, F., Giorgioni, M., Iannace, A., Mazzoli, S., Vitale, S., 2015. The role of stratabound fractures for fluid migration pathways and storage in well bedded carbonates, Ital. J. Geosci. 134, 383–395.

Guerriero, V., Mazzoli, S., Iannace, A., Vitale, S., Carravetta, A., Strauss, C., 2013. A permeability model for naturally fractured carbonate reservoirs. Mar. Petrol. Geol. 40, 115–134.

Haines, T.J., Michie, E.A.H., Neilson, J.E., Healy, D., 2016. Permeability evolution across carbonate hosted normal fault zones. Mar. Petrol. Geol. 72, 62–82.

Hausegger, S., Kurz, W., Rabitsch, R., Kiechl, E., Brosch, F., 2010. Analysis of the internal structure of a carbonate damage zone: Implications for the mechanisms of fault breccia formation and fluid flow. J. Struct. Geol. 32: 1349–1362.

Huang, N., Liu, R., Jiang, Y.J., Li, B., Yu, L.Y., 2018. Effects of fracture surface roughness and shear displacement on geometrical and hydraulic properties of three-dimensional crossed rock fracture models. Advances in Water Resources 113, 30–41.

Jia, C.Z., 1997. Tectonic characteristics and petroleum, Tarim Basin, China: Beijing：Geological Publishing House, 29–261 (in Chinese).

Kim, Y.S., Peacock, D.C.P., Sanderson, D.J., 2004. Fault damage zones. J. Struct. Geol. 26, 503–517.

Korneva, I., Tondi, E., Agosta, F., Rustichelli, A., Spina,V., Bitonte, R., Cuia, R.D., 2014. Structural properties of fractured and faulted Cretaceous platform carbonates, Murge Plateau (southern Italy). Mar. Petrol. Geol. 57, 312–326.

Li, Y., Kang, Z.J., Xue, Z.J., Zheng, S.Q., 2018. Theories and practices of carbonate

reservoirs development in China. Pet. Explor. Dev. 45, 712–722.

Li, Y.J., Zhang, Q., Zhang, G.Y., Tian, Z.J., Peng, G.X., Qiu, B., Huang, Z.B., Luo, J.C., Wen, L., Zhao, Y., Jia, T.G., 2016. Cenozoic faults and faulting phases in the western Tarim Basin (NW China): Effects of the collisions on the southern margin of the Eurasian Plate. J. Asian Earth Sci. 132, 40–57.

Liu, R.L., Li, N., Feng, Q.F., Hai. C., Wang, K.W., 2009. Application of the triple porosity model in well–log effectiveness estimation of the carbonate reservoir in Tarim oilfield. J. Petrol. Sci. Engin. 68, 40–46.

Lu, X.B., Wang, Y., Tian, F., Li, X.H., Yang, D.B., Li, T., Lv, Y.P., He, X.M., 2017. New insights into the carbonate karstic fault system and reservoir formation in the Southern Tahe area of the Tarim Basin. Mar. Petrol. Geol. 86, 587–605.

Ma, D.B., Wu, G.H., Scarselli, N., Luo, X.S., Han, J.F., Chen, Z.Y., 2019. Seismic damage zone and width–throw scaling along the strike-slip faults in the Ordovician carbonates in the Tarim Basin. Pet. Sci. 16, 752–57.

Meier, S., Bauer, J.F., Philipp, S.L., 2015. Fault zone characteristics, fracture systems and permeability implications of Middle Triassic Muschelkalk in Southwest Germany. J. Struct. Geol. 70, 170–189.

Méndez, J.N., Jin, Q., González, M., Zhang, X.D., Lobo, C., Boateng, C.D., Zambrano, M., 2020. Fracture characterization and modeling of karsted carbonate reservoirs: A case study in Tahe oilfield, Tarim Basin (western China). Mar. Petrol. Geol. 112, https://doi.org/10.1016/j.marpetgeo.2019.104104.

Micarelli, L., Benedicto, A., Wibberley, C.A.J., 2006. Structural evolution and permeability of normal fault zones in highly porous carbonate rocks. J. Struct. Geol. 28, 1214–1227.

Michie, E.A.H., 2015. Influence of host lithofacies on fault rock variation in carbonate fault zones: A case study from the Island of Malta. J. Struct. Geol. 76, 61–79.

Mitchell, T.M., Faulkner, D.R., 2009. The nature and origin of off-fault damage surrounding strike-slip fault zones with a wide range of displacements: A field study from the Atacama fault system, northern Chile. J. Struct. Geol. 31, 802–

816.

Mitchell, T.M., Faulkner, D.R., 2012. Towards quantifying the matrix permeability of fault damage zones in low porosity rocks. Earth Planet. Sci. Lett. 339–340, 24–31.

Molli, G., Cortecci, G., Vaselli, L., Ottria, G., Cortopassi, A., Dinelli, E., Mussi, M., Barbieri, M., 2010. Fault zone structure and fluid–rock interaction of a high angle normal fault in Carrara marble (NW Tuscany, Italy). J. Struct. Geol. 32, 1334–1348.

Nara, Y., Meredith, P.G., Yoneda, T., Kaneko, K., 2011. Influence of macro-fractures and micro-fractures on permeability and elastic wave velocities in basalt at elevated pressure. Tectonophysics 503, 52–59.

Neng, Y., Yang, H.J., Deng, X.L., 2018. Structural patterns of fault broken zones in carbonate rocks and their influences on petroleum accumulation in Tazhong Paleo-uplift, Tarim Basin, NW China. Pet. Explor. Dev. 45, 43–54.

O'Hara, A.P., Jacobi, R.D., Sheets, H.D., 2017. Predicting the width and average fracture frequency of damage zones using a partial least squares statistical analysis: Implications for fault zone development. J. Struct. Geol. 98, 8–52.

Olierook, H.K.H. Timms, N.E. Hamilton, P.J., 2014. Mechanisms for permeability modification in the damage zone of a normal fault, northern Perth Basin, Western Australia. Mar. Petrol. Geol. 50, 130–147.

Pang, X.Q., Tian, J., Pang, H., Xiang, C.F., Jiang, Z.X., Li, S.M., 2010. Main progress and problems in research on Ordovician hydrocarbon accumulation in the Tarim Basin. Pet. Sci. 7, 147–163.

Pei, Y., Paton, D.A., Knipe, R.J., Wu, K., 2015. A review of fault sealing behaviour and its evaluation in siliciclastic rocks. Earth-Sci. Rev. 150, 121–138.

Rotevatn, A., Bastesen, E., 2012. Fault linkage and damage zone architecture in tight carbonate rocks in the Suez Rift (Egypt): implications for permeability structure along segmented normal faults. Geol. Soc. Lond. Spec. Publ. 374, 79–95.

Savage, H.M., Brodsky, E.E., 2011. Collateral damage: Evolution with displacement of fracture distribution and secondary fault strands in fault damage zones. J. Geophys. Res. 116, B03405, doi:10.1029/2010JB007665.

Sivey, J.P., Lee, W.J., 2013. Applied well test interpretation. Society of Petroleum Engineers.

Shen, A.J., Zhao, W.Z., Hu, A.P., She, Min., Chen, Y.N., Wang, X.F., 2015. Major factors controlling the development of marine carbonate reservoirs. Petrol. Explor. Dev. 42, 597–608.

Storti, F., Balsamo, F., Cappanera, F., Tosi, G., 2011. Sub-seismic scale fracture pattern and in situ permeability data in the chalk atop of the Krempe salt ridge at Lägerdorf, NW Germany: Inferences on synfolding stress field evolution and its impact on fracture connectivity. Mar. Petrol. Geol. 28, 1315–1332.

Tang, L. J., Huang, T. Z., Qiu, H. J., Wan, G.M., Li, M., Yang, Y., Xie, D.Q., Chen, G., 2014. Fault Systems and Their Mechanisms of the Formation and Distribution of the Tarim Basin, NW China. J. Earth Sci. 25, 169–182.

Tian, F., Luo, X.R., Zhang, W., 2019. Integrated geological-geophysical characterizations of deeply buried fractured-vuggy carbonate reservoirs in Ordovician strata, Tarim Basin. Mar. Petrol. Geol. 99, 292–309.

Tondi, E., 2007. Nucleation, development and petrophysical properties of faults in carbonate grainstones: Evidence from the San Vito Lo Capo peninsula (Sicily, Italy). J. Struct. Geol. 29, 614–628.

Torabi, A., Berg, S.S., 2011. Scaling of fault attributes: A review. Mar. Petrol. Geol. 28, 1444–1460.

Torabi, A., Alaei, B., Ellingsen, T.S.S., 2018. Faults and fractures in basement rocks, their architecture, petrophysical and mechanical properties. J. Struct. Geol. 117, 256–263.

Wan, X.G., Wu, G.H., Yang, P.F., Gao, L.H., 2016. The seismic technique description of carbonate fault damage zone in Halahatang area, Tarim basin. Oil & Gas Geol. 37, 785–791 (in Chinese with English abstract).

Wan, Y.Z., Liu, Y.W., Chen, F.F., Wu, N.Y., Hu, G.W., 2018. Numerical well test model for caved carbonate reservoirs and its application in Tarim Basin, China. J. Petrol. Sci. Engin. 161, 611–624.

Wang, G., Mitchell, T.M., Meredith, P.G., Nara, Y., Wu, Z., 2016. Influence of gouge thickness and grain size on permeability of macro-fractured basalt. J. Geophys. Res. Solid Earth. http://dx.doi.org/10.1002/2016JB013363.

Wibberley, C.A.J., Shimanoto, T., 2003. Internal structure and permeability of major strike-slip fault zones: the Median Tectonic Line in Mie Prefrecture, Southwest Japan. J. Struct. Geol. 25, 59–78.

Williams, R.T., Goodwin, L..B., Mozley, P.S., 2017. Diagenetic controls on the evolution of fault-zone architecture and permeability structure: Implications for episodicity of fault-zone fluid transport in extensional basins. GSA Bull. 129: 464–478.

Wu, G.H., Gao, L.H., Zhang, Y.T., Ning, C.Z., Xie, E., 2019a. Fracture attributes in reservoir-scale carbonate fault damage zones and implications for damage zone width and growth in the deep subsurface. J. Struct. Geol. 118, 181–193.

Wu, G.H., Kim, Y.S., Su, Z., Yang, P.F., Ma, D.B., Zheng, D.M., 2020. Segment interaction and linkage evolution in a conjugate strike-slip fault system from the Tarim oilfield. Mar. Petrol. Geol. https://doi.org/10.1016/j.marpetgeo.2019.104054.

Wu, G.H., Xie, E., Zhang, Y.F., Qing, H.R., Luo, X.S., Sun, C., 2019b. Structural diagenesis in carbonate fault damage zones in the northern Tarim Basin, NW China. Minerals 9, 360; doi:10.3390/min9060360.

Wu, G.H., Yang, H.J., He, S., Cao, S.J., Liu, X., Jing, B., 2016. Effects of structural segmentation and faulting on carbonate reservoir properties: A case study from the Central Uplift of the Tarim Basin, China. Mar. Petrol. Geol. 71, 183–197.

Yang, H.J., Wu, G.H., Qing, H.R., Sun, C.H., Scarselli, N., 2020. Characterization of reservoirs, fluids and productions from the Ordovician carbonate condensate field in the Tarim Basin, NW China. in press.

Yang, H.J., Zhu, G.Y., Wang, Y., Su, J., Zhang, B., 2014. The geological characteristics of reservoirs and major controlling factors of hydrocarbon accumulation in the Ordovician of Tazhong area, Tarim Basin. Energy Explor. Exploit., 32, 345–368.

Zhang, Y.F., Tan, F., Sun, Y.B., Pan, W.Q., Wang, Z.Y., Yang, H.Q., Zhao, J.X., 2018. Differences between reservoirs in the intra-platform and platform margin reef-shoal complexes of the Upper Ordovician Lianglitag Formation in the Tazhong oil field, NW China, and corresponding exploration strategies. Mar. Petrol. Geol. 98, 66–78.

Zhao, K.Z., Zhang, L.J., Zheng, D.M., Sun, C.H., Dang, Q.N., 2015. A reserve calculation method for fracture-cavity carbonate reservoirs in Tarim Basin, NW China. Pet. Explor. Dev. 42, 277–282.

Zhao, W.Z., Shen A.J., Hu, S.Y., Zhang, B.M., Pan, W.Q., Zhou, J.G., Wang, Z.C., 2012. Geological conditions and distributional features of large-scale carbonate reservoirs onshore China. Pet. Explor. Dev. 39, 1–12.

Fig. 1. (a) The tectonic division in the Tarim Basin (the corner icon shows the location in China) (after Wu et al., 2019a); (b) the geological profile across the Tarim Basin.

Fig. 2. (a) The stratigraphic column of the Ordovician carbonate of Halahatang area; (b) the strike-slip fault system of Ordovician carbonate in the north Halahatang area, Tarim Basin (after Wu et al., 2018). Yellow area showing the envelope of the fault damage zones by AFE fracture prediction on the top of Ordovician carbonate in Halahatang area (after Wan et al., 2016).

Fig. 3. The typical strike-slip fault in seismic profiles of uninterpretated (a) and interpretated (b) (see location in Fig. 2)

Fig. 4. The photos showing typical rocks and porosity in the Ordovician carbonate in Halahatang area. (a) tight mudstone showing bedding-parallel stylolites, core; (b) dissolution pores and vugs along fractures, core; (c) grainstone showing tight cementation with micro-intragranular dissolution pores, thin section; (d) fractures and intergranular dissolution pores along fractures, thin section; (e) FMI logging image showing conjugate fractures; (f) typical cavity reservoir in logging data; (g) typical seismic section of the Ordovician carbonates (The long string of strong amplitude reflection showing “bead-shape” reflection).

Fig. 5. Photographs of fault cores. (a) calcit cement and bitumen filled fault core, core; (b) fault breccias and gouge, core; (c) multiple fillings in a cement fault core (general processes orders are: ① early stylolite; ② vertical stylolite; ③ enlarged fracture along stylolite; ④ calcite precipitation; ⑤ late microfractures; ⑥ enlarged dissolution), thin section; (d) two generations of cementation filling in microfault, later fracture in the center with open void (the pink-dye resin impregnated to show fracture porosity, after Wu et al., 2019b).

Fig. 6. Photographs of damage zones from the cores (a-d) and thin sections (e-j) (the pink-dye resin impregnated to show fracture porosity) of the Ordovician carbonates in the Halahatang area. (a) fracture networks with bitumen filling; (b) en echelon fractures filled with calcit; (c) enlarged vertical fractures; (d) fracture expansion and filling, splay micro-fractures at the tip (after Wu et al., 2019b); (e) dissolution along fractures (after Wu et al., 2019b); (f) multi-stage fractures cut-cross with the sequence from ① to ③ (after Wu et al., 2019b); (g) conjugate fractures with full calcite filling; (h) late open fracture cut across early cement enlarged fracture; (i) paralleled fractures, expansion and filling, and later fracture in the center with open void, and late micro-fractures parallel to the primary fractures; (j) calcite bridge and porosity in fracture.

Fig. 7. (a) The fracture dip angle vs. distance from fault by FMI data from 57 wells; (b) fracture dip angle histogram by FMI from 57 wells; (c) fracture aperture from FMI vs. distance from fault in the Ordovician carbonates vs. fracture angle and; (d) the average fracture frequency of a well from logging data vs. distance from fault. The average fracture frequency is the total fracture number by logging interpretation divided by the measured length in a well.

Fig. 8. (a) Porosity-permeability relation of the Ordovician limestone cores in Halahatang area. The porosity and permeability values measured from core plugs. The red cross-shapes are fracture bearing samples, and the pink lines are samples without obvious fractures; (b) average porosity and the average permeability from borehole cores vs. distance from fault in the Ordovician carbonates. The porosity and permeability data are from core plug samples.

Fig. 9. Permeability vs. porosity in lithology (a), strata (b) and oil-bearing from the core plug samples; (c) permeability vs. depth of the core plug samples.

Fig. 10. (a) Permeability vs. porosity from logging interpretation; (b) Permeability vs. porosity from same layers of core plugs (circles) and logging data (forklike) showing the heterogeneity in different scales; and porosity (c) and permeability (d) of a

reservoir zone vs. distance to fault zone from logging interpretation.

Fig. 11. (a) Oil production vs. permeability from Stoneley wave logging; (b) oil production of wells and their cumulative production vs. distance to an adjacent fault zone in the Ordovician carbonate (some data is after Wu et al., 2019a).

Figure

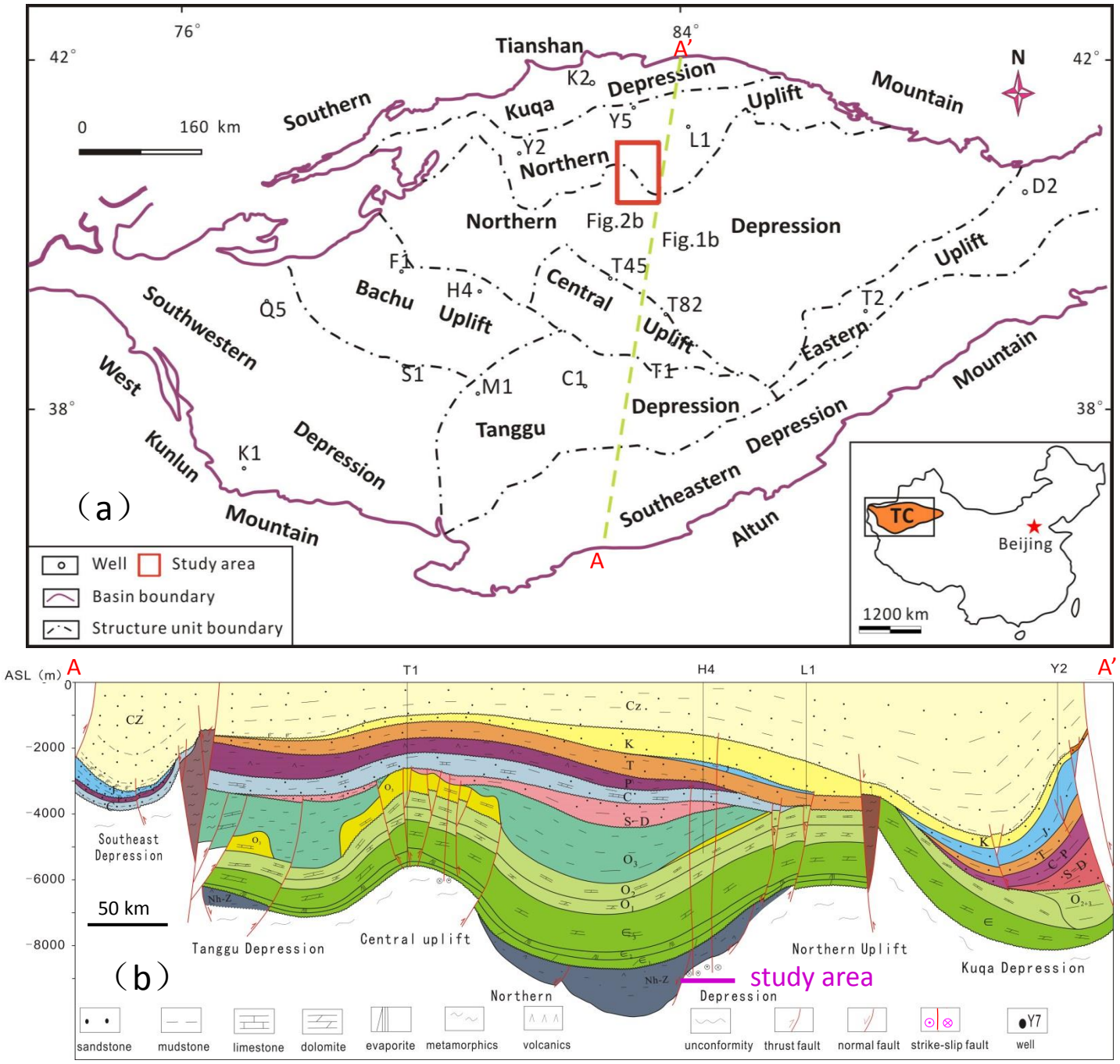
76°
84°
42°
38°
A
A'
N
0
160 km
Tianshan
Southern
Kuqa
Depression
Uplift
Mountain
Northern
Northern
Depression
Fig.2b
Fig.1b
Southwestern
Bachu
Uplift
Central
Uplift
Eastern
Uplift
West
Kunlun
Mountain
Depression
Tanggu
Depression
Depression
Southeastern
Altun
Mountain
K2
Y5
Y2
L1
D2
F1
T45
H4
T82
T2
Q5
S1
M1
C1
T1
K1
(a)
Well
Study area
Basin boundary
Structure unit boundary
TC
Beijing
1200 km
ASL (m)
0
-2000
-4000
-6000
-8000
T1
H4
L1
Y2
CZ
Cz
K
T
P
C
S-D
O3
O2
O1
Nh-Z
Southeast Depression
50 km
Tanggu Depression
Central uplift
Northern Depression
Northern Uplift
Kuqa Depression
study area
(b)
sandstone
mudstone
limestone
dolomite
evaporite
metamorphics
volcanics
unconformity
thrust fault
normal fault
strike-slip fault
well
Y7

Fig. 1

（a）

Strata		Lithological column	Lithological description
Series	Formation		
O_3	Sangtamu (O_3s) 0–400m		mudstone
	Lianglitage (O_3l) 0–150m		marlstone reef limestone bioclastic limestone calcarenite
	Tumuxiuke (O_3t) 20–30m		calcarenite
O_{1+2}	Yijianfang (O_2y) 150–200m		calcarenite bioclastic limestone reef limestone micrite limestone marlstone bioclastic limestone reef limestone
	Yingshan ($O_{1+2}y$) 500–700m		micrite limestone dolomitic limestone dolomite

reef limestone　　grainstone

（b）

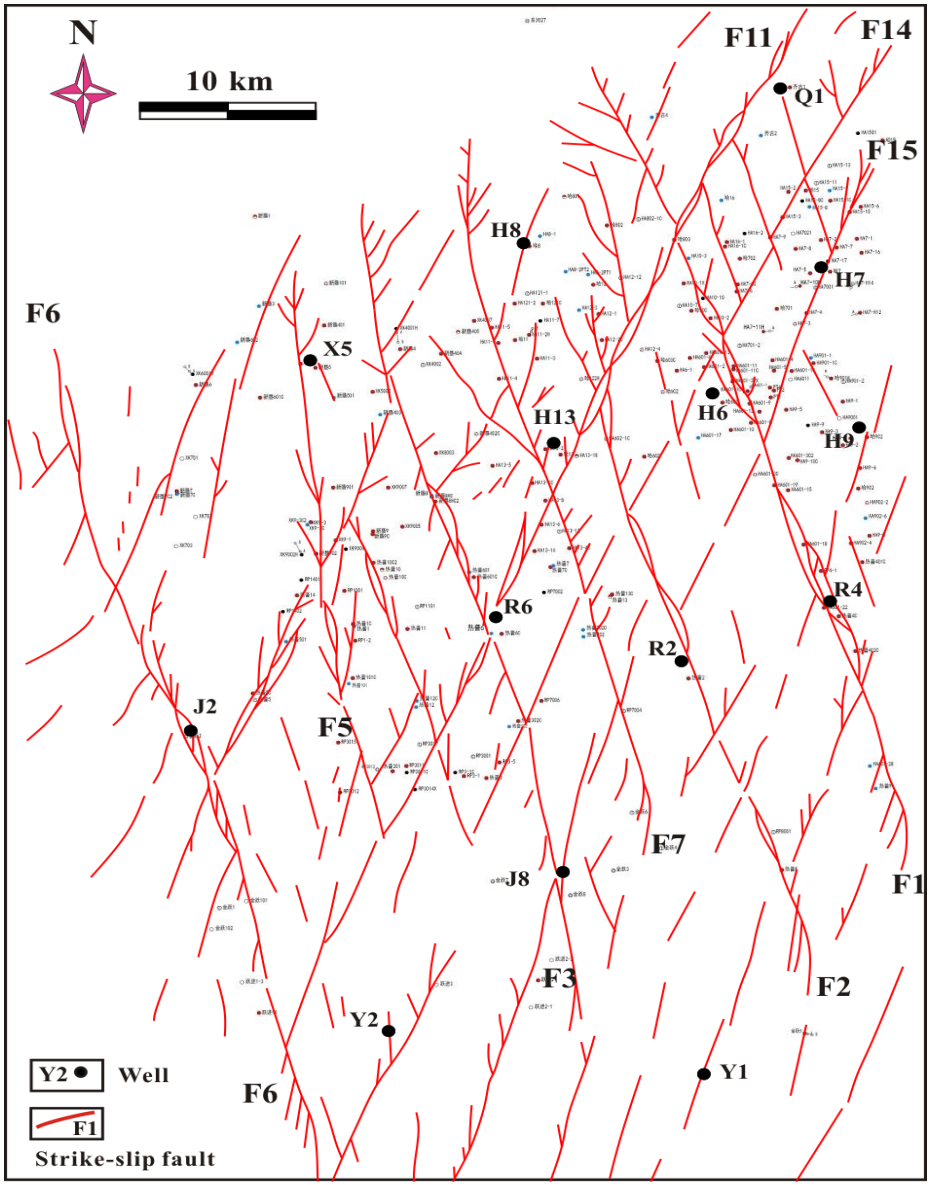

Fig. 2

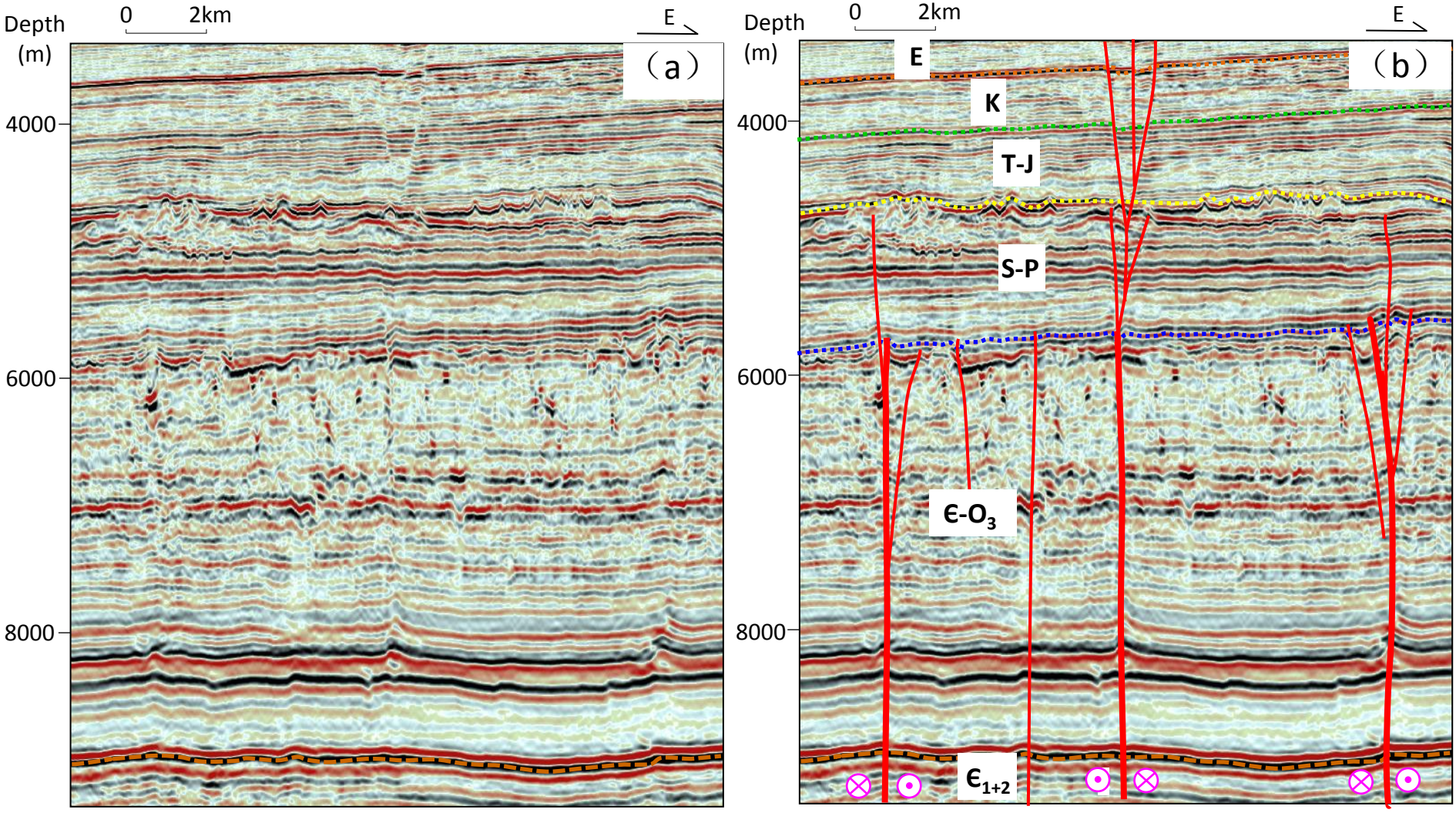
Depth
(m)
0
2km
E
(a)
4000
6000
8000
Depth
(m)
0
2km
E
(b)
E
K
T-J
S-P
Є-O3
Є1+2
4000
6000
8000

Fig. 3

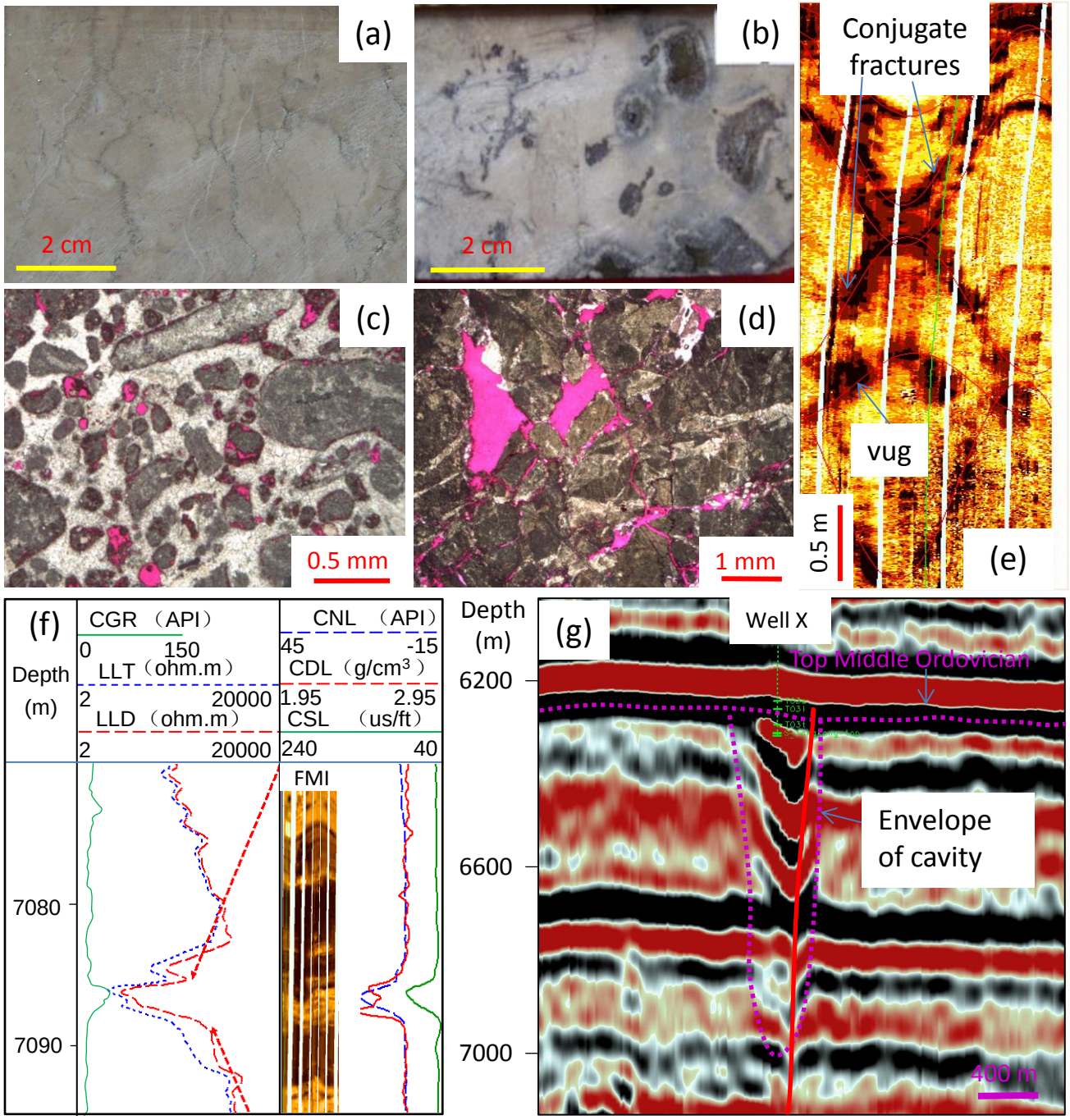
(a)
2 cm
(b)
2 cm
Conjugate fractures
vug
0.5 m
(e)
(c)
0.5 mm
(d)
1 mm
(f)
CGR （API）
0
150
LLT（ohm.m）
2
20000
LLD（ohm.m）
2
20000
CNL （API）
45
-15
CDL（g/cm³）
1.95
2.95
CSL （us/ft）
240
40
FMI
Depth (m)
7080
7090
Depth (m)
6200
6600
7000
(g)
Well X
Top Middle Ordovician
Envelope of cavity
400 m

Fig. 4

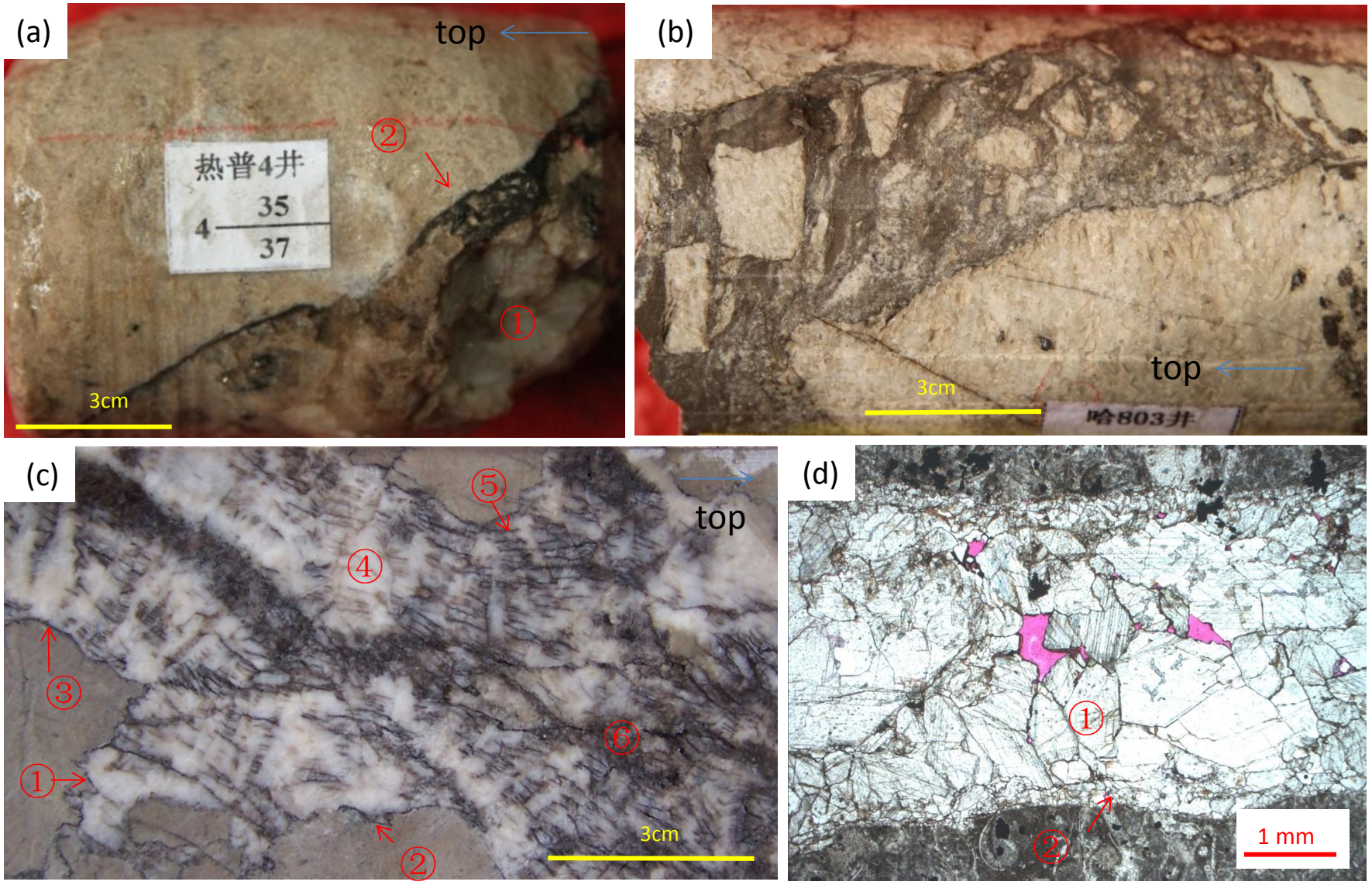

Fig. 5

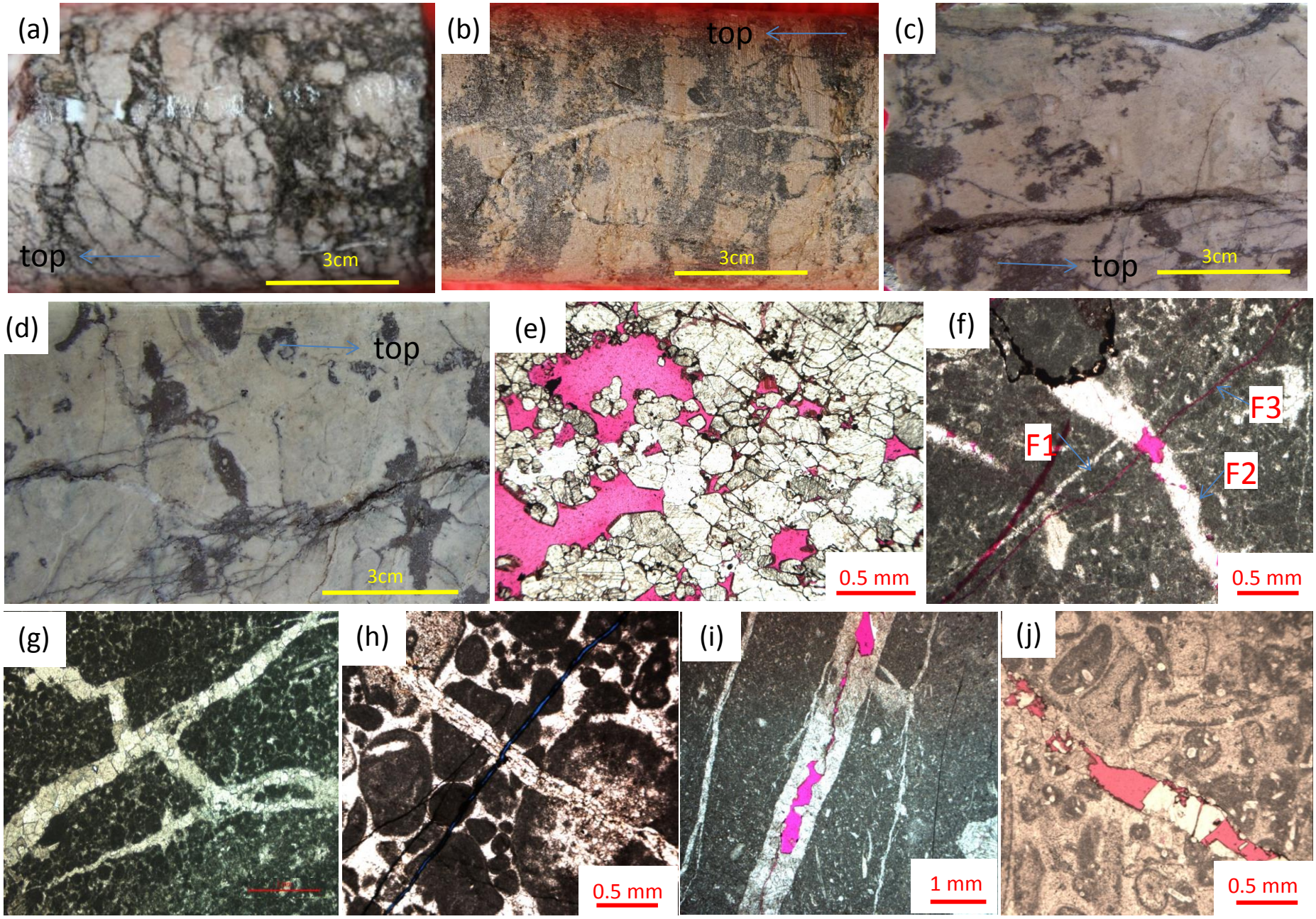
(a)
top
3cm
(b)
top
3cm
(c)
top
3cm
(d)
top
3cm
(e)
0.5 mm
(f)
F1
F2
F3
0.5 mm
(g)
(h)
0.5 mm
(i)
1 mm
(j)
0.5 mm

Fig. 6

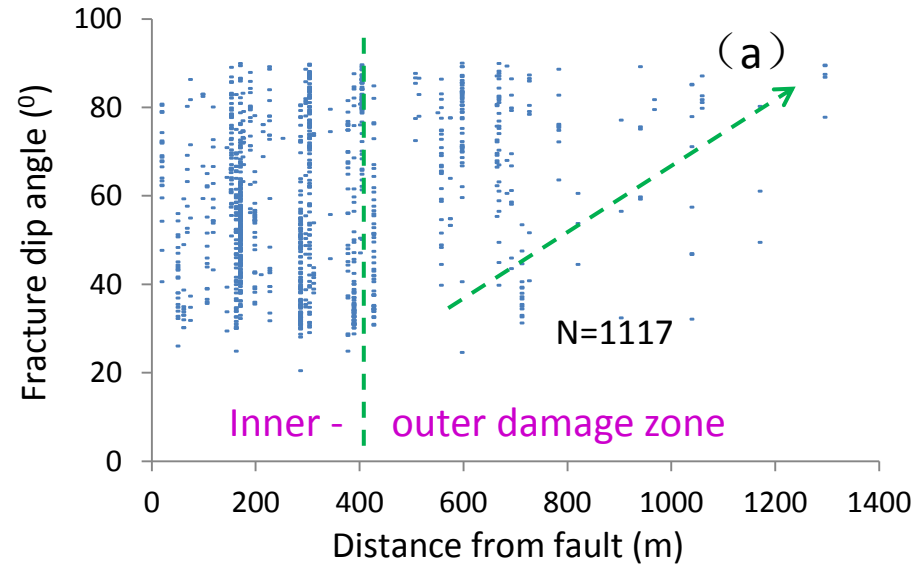
(a)
Fracture dip angle (°)
100
80
60
40
20
0
0
200
400
600
800
1000
1200
1400
Distance from fault (m)
N=1117
Inner -
outer damage zone

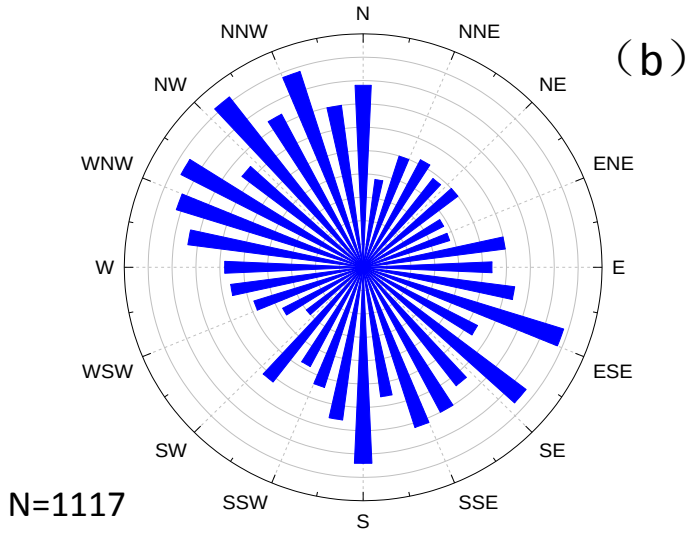
(b)
N
NNE
NE
ENE
E
ESE
SE
SSE
S
SSW
SW
WSW
W
WNW
NW
NNW
N=1117

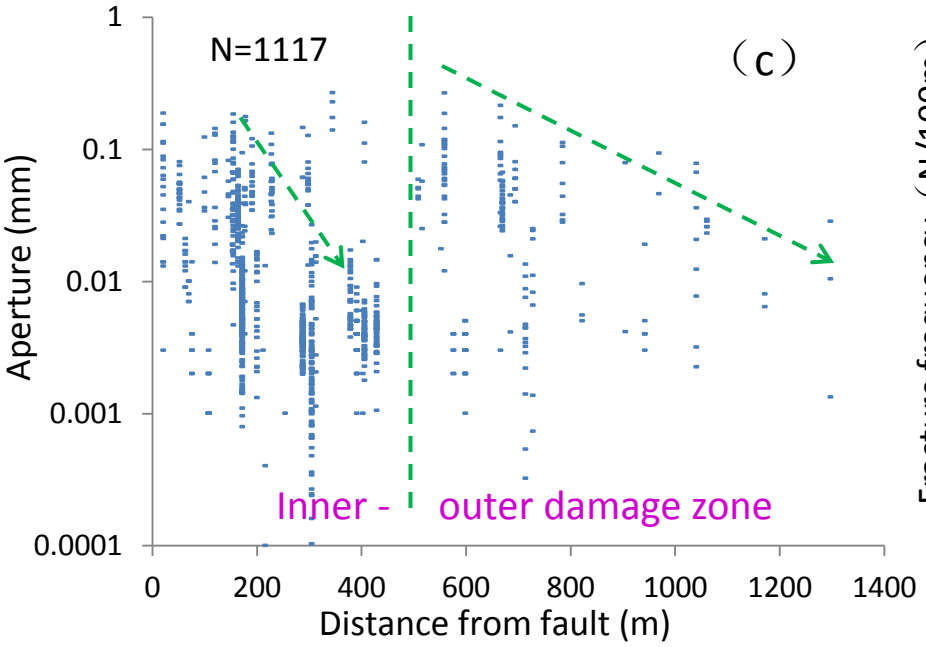
(c)
N=1117
Aperture (mm)
1
0.1
0.01
0.001
0.0001
0
200
400
600
800
1000
1200
1400
Distance from fault (m)
Inner -
outer damage zone

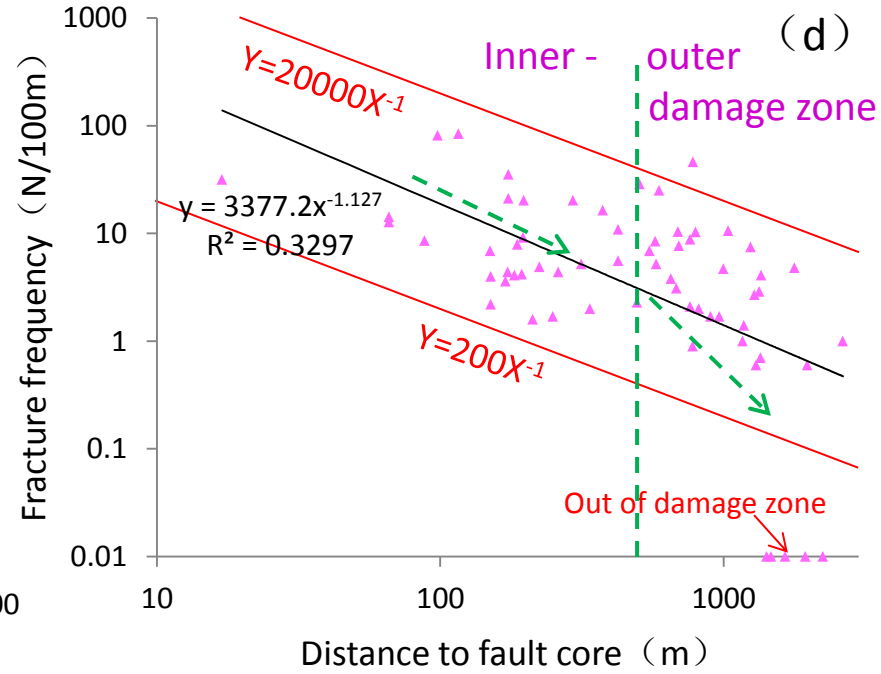
(d)
Fracture frequency (N/100m)
1000
100
10
1
0.1
0.01
10
100
1000
Distance to fault core (m)
Y=20000X-1
Y=200X-1
y = 3377.2x-1.127
R² = 0.3297
Inner -
outer
damage zone
Out of damage zone

Fig. 7

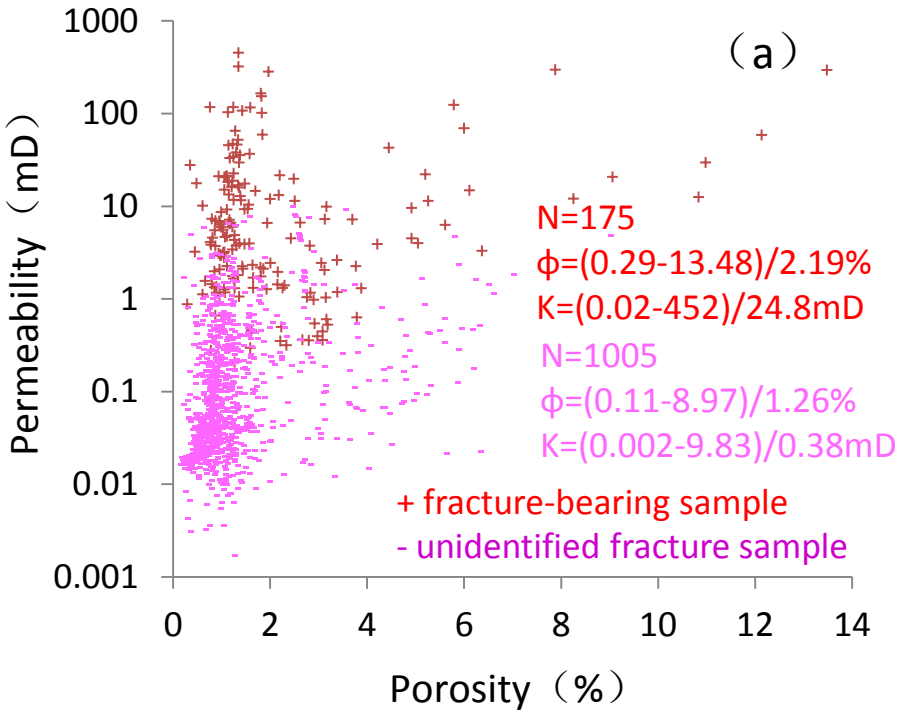
(a)
Permeability（mD）
Porosity（%）
1000
100
10
1
0.1
0.01
0.001
0
2
4
6
8
10
12
14
N=175
ϕ=(0.29-13.48)/2.19%
K=(0.02-452)/24.8mD
N=1005
ϕ=(0.11-8.97)/1.26%
K=(0.002-9.83)/0.38mD
+ fracture-bearing sample
- unidentified fracture sample

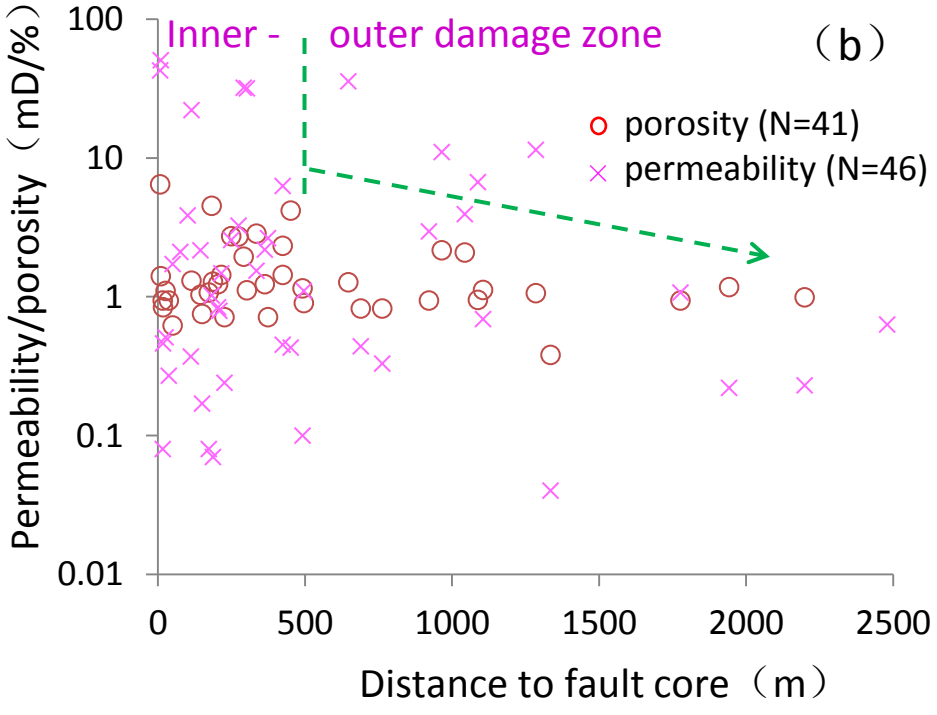
(b)
Inner - outer damage zone
Permeability/porosity（mD/%）
Distance to fault core（m）
100
10
1
0.1
0.01
0
500
1000
1500
2000
2500
porosity (N=41)
permeability (N=46)

Fig. 8

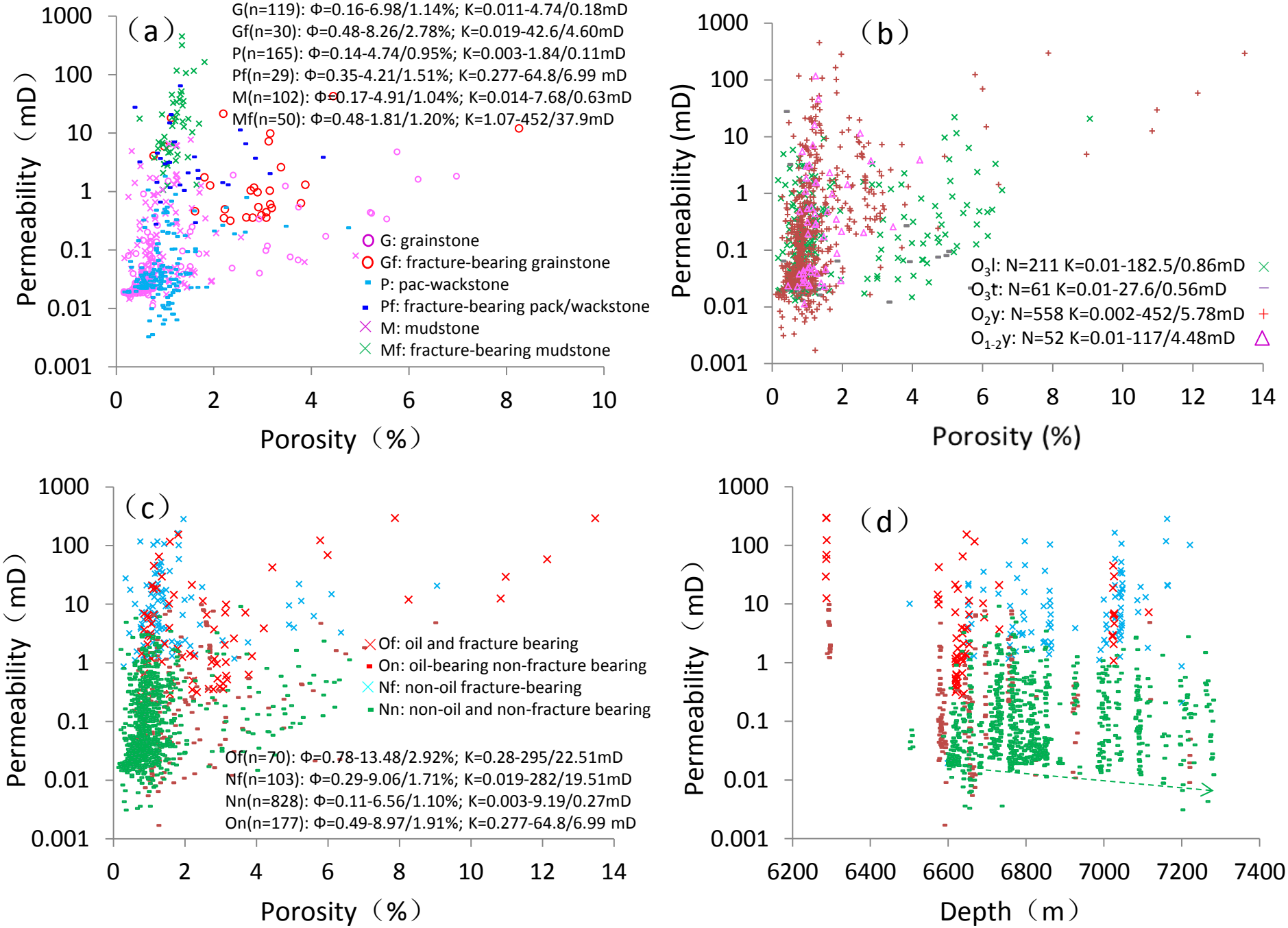
（a）
G(n=119): Φ=0.16-6.98/1.14%; K=0.011-4.74/0.18mD
Gf(n=30): Φ=0.48-8.26/2.78%; K=0.019-42.6/4.60mD
P(n=165): Φ=0.14-4.74/0.95%; K=0.003-1.84/0.11mD
Pf(n=29): Φ=0.35-4.21/1.51%; K=0.277-64.8/6.99 mD
M(n=102): Φ=0.17-4.91/1.04%; K=0.014-7.68/0.63mD
Mf(n=50): Φ=0.48-1.81/1.20%; K=1.07-452/37.9mD
G: grainstone
Gf: fracture-bearing grainstone
P: pac-wackstone
Pf: fracture-bearing pack/wackstone
M: mudstone
Mf: fracture-bearing mudstone
Permeability（mD）
Porosity（%）
（b）
O3l: N=211 K=0.01-182.5/0.86mD
O3t: N=61 K=0.01-27.6/0.56mD
O2y: N=558 K=0.002-452/5.78mD
O1-2y: N=52 K=0.01-117/4.48mD
Permeability (mD)
Porosity (%)
（c）
Of: oil and fracture bearing
On: oil-bearing non-fracture bearing
Nf: non-oil fracture-bearing
Nn: non-oil and non-fracture bearing
Of(n=70): Φ=0.78-13.48/2.92%; K=0.28-295/22.51mD
Nf(n=103): Φ=0.29-9.06/1.71%; K=0.019-282/19.51mD
Nn(n=828): Φ=0.11-6.56/1.10%; K=0.003-9.19/0.27mD
On(n=177): Φ=0.49-8.97/1.91%; K=0.277-64.8/6.99 mD
Permeability（mD）
Porosity（%）
（d）
Permeability（mD）
Depth（m）

Fig. 9

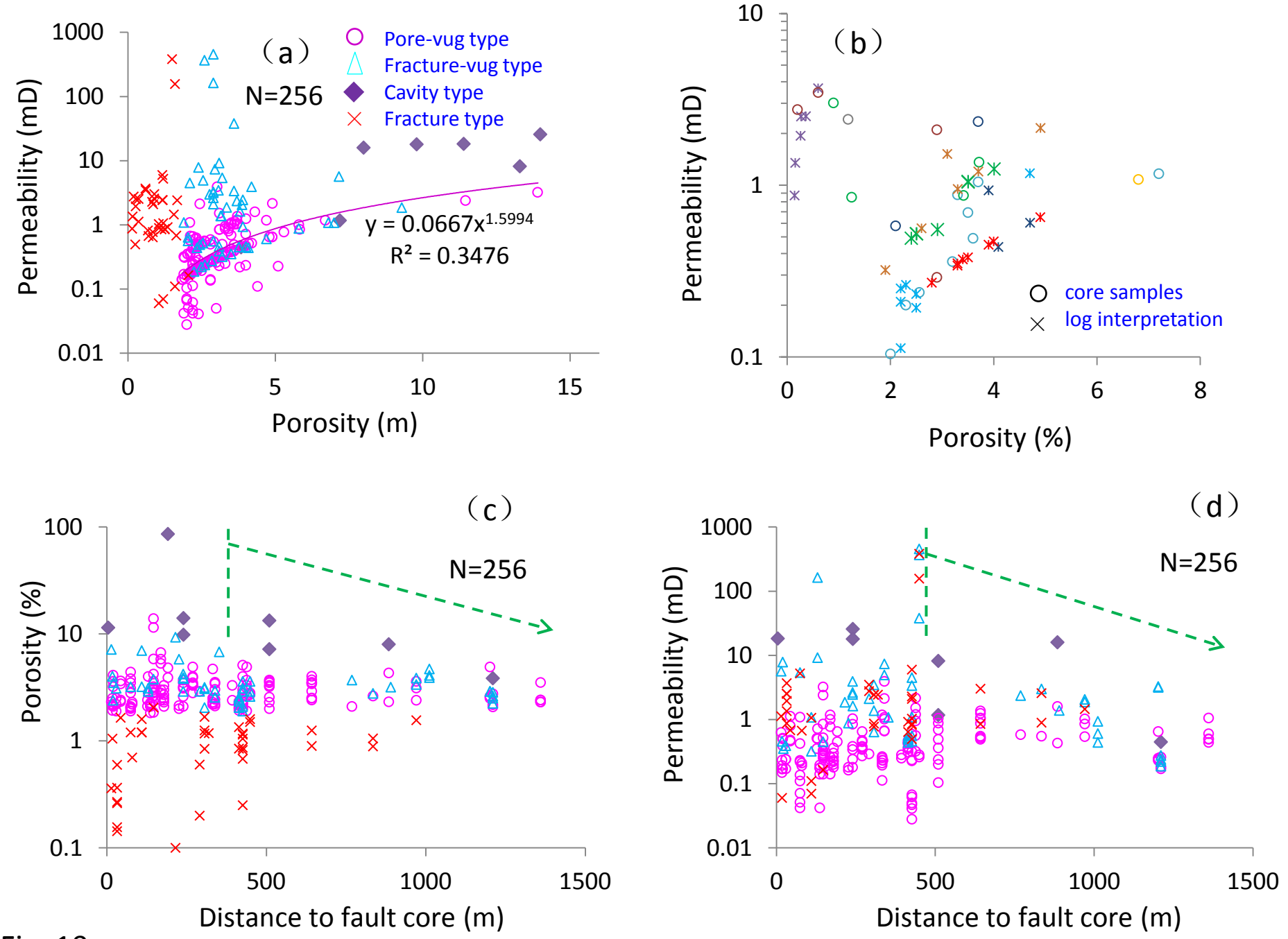
(a)
N=256
Pore-vug type
Fracture-vug type
Cavity type
Fracture type
y = 0.0667x^1.5994
R² = 0.3476
Permeability (mD)
Porosity (m)
(b)
core samples
log interpretation
Permeability (mD)
Porosity (%)
(c)
N=256
Porosity (%)
Distance to fault core (m)
(d)
N=256
Permeability (mD)
Distance to fault core (m)

Fig. 10

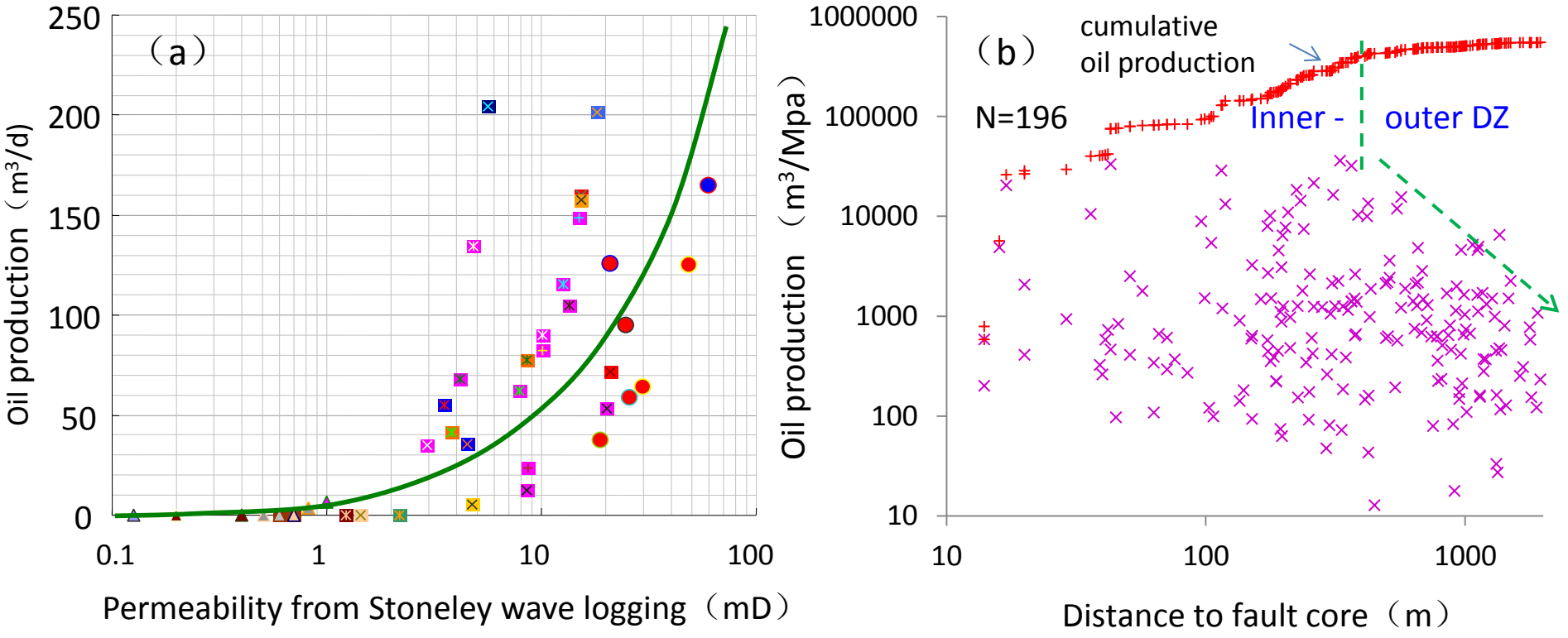
（a）
Oil production（m³/d）
250
200
150
100
50
0
0.1
1
10
100
Permeability from Stoneley wave logging（mD）
（b）
cumulative
oil production
N=196
Inner -
outer DZ
Oil production（m³/Mpa）
1000000
100000
10000
1000
100
10
10
100
1000
Distance to fault core（m）

Fig. 11

***Credit Author Statement**

Author Contributions: G.W. and J.H. conceived the study, responsible for the project administration and supervision; K.Z., H.Q., Y.Z. and Y. X. collected samples and analyzed the data; G.W., Y.Z. and H.Q. discussed and interpreted the results; G.W. and N.S. wrote the paper with contribution from all authors.